

## Nonadiabatic theory of atomic line broadening: Redistribution calculations for $\text{Sr}(^1P \leftarrow ^1S) + \text{Ar}$

P. S. Julienne and F. H. Mies

*Molecular Spectroscopy Division, National Bureau of Standards, Gaithersburg, Maryland 20899*

(Received 19 June 1986)

The close-coupled theory of collisions in a radiation field is used to calculate the absorption profile for the  $\text{Sr } ^1P \leftarrow ^1S$  resonance line broadened by collisions with Ar. The calculations predict the polarization ratios of  $\text{Sr } ^1P$  fluorescence following line wing excitation by either linear or circular polarized light. *Ab initio* calculations were used to obtain the ground and excited  $\text{SrAr}$  molecular-potential curves, which were adjusted to give improved agreement with experiment. The radiative-scattering theory gives a unified description of the absorption coefficient and polarization redistribution from the small detuning impact limit region to the far spectral wings. The cross sections for elastic and inelastic depolarizing collisions of  $\text{Sr } ^1P_1 + \text{Ar}$  were also calculated. The calculated absorption coefficient, impact-broadening rate, linear- and circular-polarization ratios, and depolarization rate coefficients are for the most part in good agreement with experiment.

### I. INTRODUCTION

Several recent papers have described experimental measurements of the collisional redistribution of polarized light by Sr or Ba perturbed by rare gases.<sup>1-4</sup> The process can be described by the following equation:

$$M(^1S_0) + A + \hbar\omega \rightarrow M(^1P_1) + A, \quad (1)$$

where  $M = \text{Sr}$  or  $\text{Ba}$  and  $A = \text{He}, \text{Ne}, \text{Ar}, \text{Kr},$  or  $\text{Xe}$ . A polarized photon of energy  $\hbar\omega$  with polarization vector  $\hat{e}_q$  is absorbed in the wings of the  $^1P \leftarrow ^1S$  pressure-broadened line ( $q=0$  for linear polarization and  $q = +1$  or  $-1$  for circular polarization). This collision-induced transition occurs during a binary collision of  $M$  and  $A$ , and may be described as a molecular transition of the transient  $MA$  quasimolecule. This excitation process can produce alignment ( $q=0, \pm 1$ ) or orientation ( $q = \pm 1$  only) of the resulting  $^1P$  atom. At a much later time the  $^1P$  atom fluoresces with photon energy near the  $^1P \rightarrow ^1S$  transition energy  $\hbar\omega_0$ . The observed polarization properties of the emitted photon depend not only on the nascent distribution of  $^1P_{1,m}$  ( $m=0, \pm 1$ ) Zeeman sublevels produced by the initial quasimolecular absorption but also on the depolarizing effect of any subsequent collisions between excitation and fluorescence. Although experiments have been carried out for strong as well as weak radiation fields,<sup>5-6</sup> we are interested here only in the case of weak fields where effects due to the dressing of the atomic states can be neglected.

A considerable body of theory on this subject has been developed recently, including complete quantum-mechanical treatments<sup>7-14</sup> and simplified models.<sup>15-20</sup> This theory has been reviewed by Burnett.<sup>21</sup> We have previously given the formal theory of polarization redistribution in weak fields in terms of the radiative scattering cross sections  $\sigma_\omega(jm)$  for process (1) and the collisional depolarization cross sections  $\sigma(jm \rightarrow jm')$ .<sup>13</sup> Preliminary results of our numerical calculations have been reported.<sup>12,19,22</sup> This paper now presents the detailed numerical results of our fully quantal close-coupling scattering cal-

culations using realistic molecular potentials for the  $\text{Sr} + \text{Ar}$  system as a prototype. Basically good agreement between measurement and theory are found for the total absorption coefficient, for the nascent  $^1P_{1,m}$  distribution for both linearly and circularly polarized light, and for the depolarization cross sections. We discuss only the numerical results here. An associated paper will show how a half-collision factorization of the radiative scattering amplitudes<sup>18-20,23</sup> can be used to project much physical insight out of these calculations. Such an analysis shows how it is possible to separate the effects of Franck-Condon excitation and axis-rotation dynamics and thereby lend qualitative credence to the simple geometric model of Lewis *et al.*<sup>15</sup>

Section II summarizes the pertinent aspects of the theory. Section III develops the molecular potentials, and Sec. IV shows our numerical data and a comparison with experiment. Our conclusions are summarized in Sec. V.

### II. THEORY

The theory needed to address this problem is the theory of collisions in a radiation field,<sup>24-27</sup> which simultaneously treats both the inelastic scattering and radiative aspects of the redistribution collision. Fully quantal scattering calculations based on such a theory have already been used to demonstrate nonadiabatic effects on spectral profiles for radiative collisions<sup>12,28</sup> and to predict observed fine-structure branching ratios for optical collisions.<sup>23,29-31</sup> Furthermore, we have shown how the angular momentum transfer theory of orientation and alignment in molecular photofragmentation<sup>32-34</sup> can be adapted to radiative scattering calculations in order to calculate polarization redistribution.<sup>13</sup> We need not give the details of the theory here but will only summarize the essential features and illustrate the content and structure of the coupled equations.

### A. Reduced coupled equations

The perturber atom is a structureless  $^1S_0$  atom, whereas the  $M$  atom has angular momentum  $j_0=0$  and  $j=1$  in its respective initial and final states. The presence of the radiation field of polarization  $\hat{\mathbf{e}}_q$  imposes a preferred direction in space for angular momentum quantization. The quantization  $z$  axis is taken to be along  $\hat{\mathbf{e}}_q$  for linearly polarized light and along the propagation direction of light for circularly polarized light. The scattering channel states which describe the asymptotic fragments with atomic angular momentum  $j$  and relative angular momentum  $l$  are written as eigenstates of total angular momentum  $\mathbf{J}=\mathbf{l}+\mathbf{j}$  in order to use the symmetry properties of molecular eigenfunctions,

$$|ljJM\rangle = \sum_{m_l, m} (ljJ | m_l m M | l m_l \rangle | j m \rangle). \quad (2)$$

The channel states span all internal and relative coordinates except the magnitude of the internuclear separation  $R$  and form a convenient basis, the Hund's case-( $e$ ) basis, for expanding the coupled equations for the radial amplitudes. The case-( $e$ ) basis functions have well-defined molecular parity with respect to inversion of all coordinates (electrons, nuclei) through the molecular center of mass. The standard molecular spectroscopic parity labels<sup>35</sup> are  $e$  and  $f$  for the respective basis functions of parity  $(-1)^J$  and  $-(-1)^J$ .

The construction of the coupled equations for field-free scattering in the case-( $e$ ) basis follows standard procedures.<sup>24,29,36</sup> For the present problem the field-free close-coupling expansion for each  $j$  and  $J$ ,

$$\Psi(jJ) = \sum_l |ljJM\rangle F(ljJ; R) / R, \quad (3)$$

generates the following coupled equation(s):

$$\frac{d^2}{dR^2} \underline{F} + \frac{2\mu}{\hbar^2} [E \cdot \underline{1}^0 - \underline{V}(R)] \underline{F} = \underline{0}. \quad (4)$$

The nonvanishing coupling matrix elements of  $\underline{V}$  are

shown in Table I. The Born-Oppenheimer potentials  $W_1$ ,  $W_2$ , and  $W_3$  in Table I are defined to vanish as  $R \rightarrow \infty$ . The matrix elements  $V_{ll'}(R)$  in Table I are indexed by the permitted values of channel-state quantum numbers  $l$  defined by Eq. (2) for a given total angular momentum  $J$ . The nondegenerate  $X^1\Sigma$  initial state of  $e$  parity, for which only  $l_0=J_0$  is permitted, is thus described by a single scattering equation. The  $3 \times 3$   $\underline{V}$  matrix for the threefold degenerate set of final states for a given  $J$  separates into two blocks of opposite parity: a  $1 \times 1$  block for the  $A^1\Pi$  state of  $f$  parity with  $l=J$  and a  $2 \times 2$  block for the  $B^1\Sigma$  and  $A^1\Pi$  states of  $e$  parity with  $l=J \pm 1$ . Solution of the coupled equations defined by substituting  $\underline{V}$  from Table I into Eq. (4) completely defines the ground-state elastic and excited-state elastic and depolarizing cross sections for field-free collisions (see Sec. IID below). Note that the equations for field-free scattering do not depend on the quantum number  $M$ , that is, on the direction of  $\mathbf{J}$  in space.

When the molecule-field states<sup>24-27</sup> are used as a basis for the coupled system, molecule plus radiation, these equations must be modified to take into account the new interactions introduced by the radiation field. First, the excited state energy in Table I must be decreased by  $\hbar\omega$ , since one less photon is present after an absorption event. The electronic-field asymptotic energy is chosen to be 0 for the ground state and is  $-\Delta$  for the excited state, where

$$\Delta = \hbar\omega - \hbar\omega_0 \quad (5)$$

is the detuning. Second, the coupled equations must be expanded to account for the new interactions introduced by the dipolar coupling with the field<sup>24</sup>

$$V^{\text{rad}} = (2\pi\hbar\omega\phi/c)^{1/2} \hat{\mathbf{e}}_q \cdot \mathbf{d}, \quad (6)$$

where  $\phi$  is the field intensity (photons  $\text{cm}^{-2} \text{sec}^{-1}$ ) and  $\mathbf{d}$  is the molecular dipole operator. The following selection rules apply to the matrix elements of  $V^{\text{rad}}$ :

TABLE I. Nonradiative matrix elements of  $V(R)$ .  $B(R) = \hbar^2/2\mu R^2$ .  $W_1(R)$ ,  $W_2(R)$ ,  $W_3(R) = X^1\Sigma$ ,  $A^1\Pi$ , and  $B^1\Sigma$  potentials, respectively.  $\hbar\omega_0 = E_{Sr}(^1P) - E_{Sr}(^1S)$ .

$^1S + ^1S$ $e$ parity	
$l_0 = J_0$	$W_1(R) + BJ_0(J_0 + 1)$
$^1P + ^1S$ $f$ parity	
$l = J$	$W_2(R) + BJ(J + 1) + \hbar\omega_0$
	$^1P + ^1S$ $e$ parity
	$l = J - 1$ <span style="float: right;"><math>l = J + 1</math></span>
$l = J - 1$	$\frac{J}{2J + 1} W_3 + \frac{J + 1}{2J + 1} W_2 + BJ(J - 1) + \hbar\omega_0$
$l = J + 1$	$\frac{[J(J + 1)]^{1/2}}{2J + 1} (W_2 - W_3)$
	$\frac{J + 1}{2J + 1} W_3 + \frac{J}{2J + 1} W_2 + B(J + 1)(J + 2) + \hbar\omega_0$

$$J = J_0 + b ,$$

$$M = M_0 + q ,$$

$$p = -p_0 ,$$

where  $p$  designates parity. The three possible values of the branch index  $b$ ,  $-1, 0, +1$ , designate respective  $P$ ,  $Q$ , and  $R$  transitions, in accordance with the nomenclature of molecular spectroscopy. The selection rules limit radiation-induced transitions from the  $e$ -parity initial state of total angular momentum  $J_0$  to the following:

(1)  $P$  transitions to the two coupled final  $e$ -parity states with  $J = J_0 - 1$ ,

(2)  $Q$  transitions to the single final  $f$ -parity state with  $J = J_0$ ,

(3)  $R$  transitions to the two coupled final  $e$ -parity states with  $J = J_0 + 1$ . Thus, the complete  $M + A$  radiative scattering problem can be solved by setting up the six coupled equations in accordance with this scheme. This set describes the initial state and the five possible final channels accessible from the initial state.

Although the  $V^{\text{rad}}$  matrix elements in Eq. (6) depend on  $M$  and  $q$ , Ref. 13 shows how for weak radiation fields this dependence can be eliminated from the coupled equations by introducing reduced radiative coupling matrix elements,

$$d^{(1)}(l_j J \leftarrow l_0 j_0 J_0) = \frac{\langle l_j J M | \hat{\mathbf{e}}_q \cdot \mathbf{d} | l_0 j_0 J_0 M_0 \rangle}{(J_1 J_0 | M, -q)} . \quad (7)$$

If we neglect the  $R$  dependence of the electronic transition dipole moment, the reduced matrix elements due to the nonvanishing asymptotic atomic transition moment are

$$d^{(1)} = (-1)^a \delta_{ll_0} (2j+1)^{1/2} (2J+1)^{1/2} \times W(j_0 j J_0 J; 1 l_0) (j || d || j_0) , \quad (8)$$

where  $W$  is a Racah coefficient and the phase is given by

$$a = 1 + q + j + l - 3J . \quad (9)$$

The reduced radiative coupling matrix elements that appear in the coupled equations are

$$V^{\text{rad}}(\text{cm}^{-1}) = (2\pi \hbar \omega \phi / c)^{1/2} d^{(1)} = 5.8578 \times 10^{-4} \phi_w^{1/2} d^{(1)} , \quad (10)$$

where  $\phi_w$  is laser power in  $\text{W cm}^{-2}$  and  $d^{(1)}$  from Eq. (8) is in atomic units ( $ea_0$ ). The reduced atomic matrix element  $(j || d || j_0)$  for  $\text{Sr } ^1P \leftarrow ^1S$  is  $3.12 ea_0$ , based on a measured absorption oscillator strength of 1.92.<sup>37</sup>

Note that Eq. (8) exhibits the Hund's case ( $e$ ) selection rule  $l = l_0$ . This corresponds to our physical picture that at large internuclear separation the photon can only cause a change in the atomic angular momentum  $j$ , not in the relative angular momentum of nuclear motion  $l$ . However, if the  $R$ -dependent interatomic interaction is taken into account, additional  $R$ -dependent terms in the molecular transition dipoles appear. These long-range  $R$ -dependent terms vary as  $R^{-3}$  and have the selection rules  $l = l_0, l_0 \pm 2$ . Although the presence of these  $R$ -dependent induced-moment terms with  $l \neq l_0$  can have a large influence on the spectral profile for asymptotically forbidden transitions,<sup>12,28</sup> they are of little consequence for the case of optical collisions. The long-range case- $(e)$  reduced transition dipoles may be written as

$$d^{(1)}(J l \leftarrow J_0 l_0) = (j || d || j_0) [C_0(J l \leftarrow J_0 l_0) + C_3(J l \leftarrow J_0 l_0) \alpha / R^3] , \quad (11)$$

where  $\alpha$  is the polarizability of the Ar atom. The expressions for  $C_0$  and  $C_3$  are shown in Table II. Since the  $R$ -dependent terms only amount to a few percent at most for the relevant range of  $R$  for  $\text{Sr} + \text{Ar}$ , the  $C_3$  terms will be neglected here in our numerical calculations.

## B. Reduced scattering matrix elements

The six coupled equations are readily constructed using the molecular electronic-rotational matrix elements in Table I and the reduced radiative coupling matrix elements of Eqs. (10) and (11) and Table II. These equations do not depend on radiation polarization  $q$  or space projection  $M$  of  $J$ . Since reduced-coupling matrix elements are used in the coupled equations, the desired reduced  $s_w$  matrix elements,<sup>13</sup> which describe either linearly or circularly

TABLE II. Radiative coupling coefficients of Eq. (11).

Transition	$C_0$	$C_3$
$P \ l = J_0 - 2$	0	$3 \left[ \frac{J_0(J_0 - 1)}{(2J_0 - 1)(2J_0 + 1)} \right]^{1/2}$
$P \ l = J_0$	$-\left[ \frac{2J_0 - 1}{2J_0 + 1} \right]^{1/2}$	$-\frac{J_0 + 1}{[(2J_0 - 1)(2J_0 + 1)]^{1/2}}$
$Q \ l = J_0$	1	-1
$R \ l = J_0$	$-\left[ \frac{2J_0 + 3}{2J_0 + 1} \right]^{1/2}$	$-\frac{J_0}{[(2J_0 + 1)(2J_0 + 3)]^{1/2}}$
$R \ l = J_0 + 2$	0	$3 \left[ \frac{(J_0 + 1)(J_0 + 2)}{(2J_0 + 1)(2J_0 + 3)} \right]^{1/2}$

polarized light experiments, are directly obtained when the  $S$  matrix in the asymptotic case-( $e$ ) basis is extracted from the asymptotic close-coupled solutions in accordance with the normal procedures of scattering theory.

The angular momentum transfer formalism of Ref. 13, summarized in Sec. II C below, applies only when the radiation field is sufficiently weak that radiative couplings produce a small perturbation on the colliding atoms, i.e.,  $|s_\omega| \ll 1$ . The required condition is that the detuning  $\Delta$  be large compared to  $\hbar\Omega$ ,<sup>13,39</sup> where the Rabi frequency  $\Omega$  for the  $^1P \leftarrow ^1S$  transition is given by<sup>24</sup>

$$\hbar\Omega = (8\pi\hbar\omega\phi/c)^{1/2}(j||d||j_0). \quad (12)$$

It is this requirement that the field be weak which ensures that the  $s_\omega$  are linear in  $V^{\text{rad}}$  so that the dependence on  $q$  and  $M$  can be factored using the Wigner-Eckart theorem and incorporated analytically into the algebra. For strong fields the explicit dependence on  $q$  and  $M$  needs to be taken into account. DeVries and George<sup>27</sup> have suggested that for strong fields the Clebsch-Gordon coefficient  $(J_1J_0|M, -q)$  in the radiative coupling matrix element can be replaced by its mean value  $1/\sqrt{3}$ . Although this approximation is convenient for estimating the total cross section for strong-field cell experiments,<sup>38</sup> it is not suitable for calculating polarization redistribution in strong fields.

Even for weak fields there are certain subtleties involved in extracting the case-( $e$ )  $S$ -matrix elements from the numerical solutions of the coupled radiative scattering equations. The problem arises for optical collisions since there are nondiagonal radiative coupling terms in the asymptotic potential matrix. Thus, the proper asymptotic states for calculating the  $S$  matrix are the diagonalized, or dressed, channel states, not the field-free case-( $e$ ) channel states. However, we have used dressed-atom scattering theory to show that the small perturbative effect of dressing can be ignored for weak fields, i.e., when  $\hbar\Omega \ll \Delta$ .<sup>39</sup> To first order in the radiative coupling, the radiative  $S$ -matrix elements in either the dressed or undressed bases are the same and are proportional to the nonadiabatic Franck-Condon-type matrix elements,

$$\begin{aligned} s_\omega(ljJ \leftarrow l_0j_0J_0) &\equiv s_\omega^b(lJ_0) \\ &= -2\pi i (2\pi\hbar\omega\phi/c)^{1/2} \\ &\quad \times \langle \Psi^-(ljJ) | d^{(1)} | \Psi^+(l_0j_0J_0) \rangle \end{aligned} \quad (13)$$

where  $\Psi^+$  and  $\Psi^-$  are field-free scattering wave functions with respective incoming and outgoing scattering boundary conditions (see Refs. 13 and 39 for details). Some of the practical consequences of asymptotic dressing are discussed in Sec. IV.

Note that the  $s_\omega$  in Eq. (13) are proportional to  $\phi^{1/2}$ , which serves as a scaling parameter in the calculations. As long as  $\phi$  is not too large,  $s_\omega/\phi^{1/2}$  is a constant independent of  $\phi$ . The observable absorption coefficient and polarization ratios described below are thus independent of the choice of  $\phi$ .

### C. Radiative scattering cross section

The radiative scattering cross sections  $\sigma_\omega(jmq)$  for producing the excited state in Zeeman sublevel  $m$  when excit-

ed by photons of polarization  $q$  are given by<sup>13</sup>

$$\sigma_\omega(jmq) = \sum_{t=0}^2 \frac{3(j_1t|m, -q)^2}{2t+1} \sigma_\omega^t(j). \quad (14)$$

This equation applies to a cell experiment where there is a random spatial distribution of  $\mathbf{J}$  vectors, i.e., a micro-canonical distribution of  $M$ . The transfer cross sections  $\sigma^t$  for the Sr + Ar system ( $l_0 = J_0$ ) are defined by

$$\sigma_\omega^t(j) = \frac{\pi}{k^2} \sum_{J_0} \frac{2J_0+1}{3(2j_0+1)} \sum_l |p^t(lJ_0\varepsilon_0)|^2, \quad (15)$$

where  $p^t$  is given by the following coherent sum over reduced radiative matrix elements:

$$\begin{aligned} p^t(lJ_0\varepsilon_0) &= \sum_{b=-1}^1 (2J+1)^{1/2}(2t+1)^{1/2} \\ &\quad \times W(l, j, J_0, 1; J, t) s_\omega^b(lJ_0\varepsilon_0). \end{aligned} \quad (16a)$$

The radiative matrix elements  $s_\omega$  are uniquely defined by the following indices:  $\varepsilon_0 = \hbar^2 k^2 / 2\mu$ , the incident collision kinetic energy;  $\omega$ , the photon frequency (or, equivalently, the detuning  $\Delta$ );  $J_0$ , the initial angular momentum;  $b$ , the branch index; and  $l$ , the final relative angular momentum of the separating atoms. When the coupled equations are solved numerically for a given choice of  $\varepsilon_0$ ,  $\Delta$ , and  $J_0$ , five radiative  $S$ -matrix elements are found corresponding to the permitted combinations of  $b$  and  $l$ . If Eq. (14) is written as

$$p^t(lJ_0) = \sum_b C_{tb}(lJ_0) s_\omega^b(lJ_0), \quad (16b)$$

then Table III shows the coefficients in the expansion (16b).

The total cross section  $\sigma_\omega(j)$  for producing the final state  $j$  irrespective of  $m$  is readily shown to be

$$\sigma_\omega = \sum_{t=0}^2 \sigma_\omega^t. \quad (17)$$

The index  $j$  for the cross sections will often be dropped, since only the  $j=1$   $^1P$  final state is excited. The total cross section can also be written as

$$\sigma_\omega = \sum_{b=-1}^{+1} \sigma_\omega^b, \quad (18)$$

by introducing the branch partial cross sections

$$\sigma_\omega^b = \frac{\pi}{k^2} \sum_{J_0} \frac{(2J_0+1)}{3(2j_0+1)} \sum_l |s_\omega^b(lJ_0\varepsilon_0)|^2. \quad (19)$$

Equation (16) shows that the final-state distribution depends on the coherent mixture of final states resulting from separate  $P$ ,  $Q$ , and  $R$  excitation followed by independent dynamical evolution to the asymptotic states. On the other hand, Eq. (19) shows that the total cross section depends only on an incoherent sum of the individual matrix elements. The total cross section, which is independent of  $q$ , can also be written as

$$\sigma_\omega = \sum_{m=-j}^j \sigma_\omega(jmq). \quad (20)$$

TABLE III.  $C_{ib}(J_0)$  coefficients of Eq. (16b).

$t$	$l$	$b = -1$ (P)	$b = 0$ (Q)	$b = 1$ (R)
0	$J_0 - 2$	0	0	0
1	$J_0 - 2$	0	0	0
2	$J_0 - 2$	$\left[ \frac{2J+1}{5} \right]^{1/2}$	0	0
0	$J_0$	$\left[ \frac{2J_0-1}{3} \right]^{1/2}$	$-\left[ \frac{2J_0+1}{3} \right]^{1/2}$	$\left[ \frac{2J_0+3}{3} \right]^{1/2}$
1	$J_0$	$-\left[ \frac{(2J_0-1)(J_0+1)}{6J_0} \right]^{1/2}$	$\left[ \frac{2J_0+1}{6J_0(J_0+1)} \right]^{1/2}$	$\left[ \frac{J_0(2J_0+3)}{6(J_0+1)} \right]^{1/2}$
2	$J_0$	$\left[ \frac{(2J_0+3)(J_0+1)}{30J_0} \right]^{1/2}$	$\left[ \frac{(2J_0-1)(2J_0+1)(2J_0+3)}{30J_0(J_0+1)} \right]^{1/2}$	$\left[ \frac{J_0(2J_0-1)}{30(J_0+1)} \right]^{1/2}$
0	$J_0 + 2$	0	0	0
1	$J_0 + 2$	0	0	0
2	$J_0 + 2$	$\left[ \frac{2J_0+1}{5} \right]^{1/2}$	0	0

Equations (17)–(20) give useful sum rules for checking the numerical results.

#### D. Spectral profile

The total radiative scattering cross section  $\sigma_\omega$  can be related to observable features of the spectrum. Let us first define the second-order rate coefficient for radiative scattering,

$$k_\omega = \langle \sigma_\omega v \rangle, \quad (21)$$

where  $v$  is relative collision velocity and the angle brackets indicate an average over the thermal velocity distribution. If the detuning is in the far spectral wings of the profile where the one-perturber approximation applies, the total rate of converting reactants to products,  $[M][A]k_\omega$ , where the square brackets indicate number density, is the same as the rate of disappearance of photons  $\alpha_\omega\phi$ , where  $\alpha_\omega$  is the Beer's law absorption coefficient. Thus, in the far spectral wings the normalized absorption coefficient  $K_\omega$  in units of  $\text{cm}^5$  is<sup>13</sup>

$$K_\omega = \frac{\alpha_\omega}{[M][A]} = k_\omega / \phi. \quad (22)$$

The right-hand side of this equation is actually independent of  $\phi$ , which cancels due to the proportionality of  $k_\omega$  to  $\phi$ .

Let us define the quantity

$$\gamma_E(\Delta) = \frac{2\Delta^2}{\hbar^2\Omega^2} k_\omega[A], \quad (23)$$

which has the units  $\text{sec}^{-1}$  of a first-order rate coefficient. It can be shown that the standard expression<sup>40–42</sup> for the pressure-broadening rate (or width in frequency units) in the impact limit for an isolated line may be written as

$$\gamma_E(0) = \lim_{\Delta \rightarrow 0} \gamma_E(\Delta), \quad (24)$$

where the condition  $V^{\text{rad}} \ll \Delta$  must be satisfied while taking the limit. This quantity is nonvanishing in the impact limit since  $\sigma_\omega$  varies as  $\Delta^{-2}$  in this limit. The impact-limit absorption profile is

$$I(\Delta) = \frac{1}{\pi} \frac{\gamma_n + \gamma_E(0)}{(\omega - \omega_0 - \delta)^2 + [\gamma_n + \gamma_E(0)]^2}, \quad (25)$$

where  $\gamma_n$  is the natural broadening rate and  $\delta$  is the usual shift term. We will defer to a separate paper any detailed discussion of the radiative scattering impact-limit theory. However, the result in Eqs. (23)–(24) is readily derived by comparing the standard result<sup>40–42</sup> with the  $\sigma_\omega$  found by applying the impact-limit analysis<sup>18,43</sup> to the close-coupled Franck-Condon amplitude on the right-hand side of Eq. (13). The results in Eqs. (23)–(25) are rigorous for the isolated  $^1P \leftarrow ^1S$  line and include the effect of both elastic and inelastic (depolarizing) collisions.

A simple steady-state kinetic model shows that the total rate of fluorescence  $R_F$  (photons  $\text{cm}^{-2} \text{sec}^{-1}$ ) from the excited  $^1P$  state is just equal to the radiative excitation rate  $[M][A]k_\omega$ . We see immediately by rewriting Eq. (23) that

$$R_F = \gamma_E(\Delta)[M] \frac{\hbar^2\Omega^2}{2\Delta^2}. \quad (26)$$

Equation (26) is equivalent to the expressions introduced by Lisista and Yakovlenko<sup>44</sup> and Cooper,<sup>7</sup> which have been used to interpret the integrated intensity of the  $^1P$  fluorescence following wing  $^1P \leftarrow ^1S$  excitation in experiments on Sr + Ar<sup>6</sup> and Ca + He.<sup>45</sup> The first-order rate coefficient  $\gamma_E(\Delta)$  is interpreted as a frequency-dependent broadening rate which approaches the impact-limit result, Eq. (24), for small detuning and is proportional to the normalized absorption coefficient, Eq. (22), for large detuning,

$$\gamma_E(\Delta) = \frac{2\Delta^2}{\hbar^2\Omega^2} \phi[A]K_\omega. \quad (27)$$

The density dependence can be eliminated from  $\gamma_E(\Delta)$  to define a frequency-dependent broadening rate coefficient  $k_E(\Delta)$  by

$$k_E(\Delta) = \gamma_E(\Delta)/[A] = \frac{2\Delta^2}{\hbar^2\Omega^2} k_\omega. \quad (28)$$

The function  $k_E(\Delta)$  is useful to plot in that it is defined throughout the profile from the core to the far wings, it varies much less rapidly with  $\Delta$  than the radiative scattering rate coefficient  $k_\omega$ , and it prominently exhibits satellite features.

Before leaving this discussion of the total cross section, it is instructive to note the relation to the unified Franck-Condon (UFC) theory for the absorption profile.<sup>46</sup> The major approximation of the Szudy-Baylis UFC theory<sup>46</sup> is to make the adiabatic approximation, which ignores couplings between different molecular Born-Oppenheimer states so that motion occurs only on single Born-Oppenheimer, or adiabatic, molecular potentials. The adiabatic theory requires that the single-channel wave functions of the Born-Oppenheimer molecular potentials be used to evaluate the Franck-Condon matrix elements in Eq. (13) instead of using the close-coupled scattering wave functions. The equivalent adiabatic approximation is introduced into the radiative scattering calculation by ignoring any off-diagonal nonradiative mixing terms in the coupling potential matrix  $V$  and using only the molecular Born-Oppenheimer potentials as diagonal scattering potentials for the initial and final scattering states.<sup>28</sup> [For the present problem this requires a Hund's case-(a) basis and neglect of the  $^1\Sigma$ - $^1\Pi$  Coriolis coupling.] Such a calculation gives adiabatic  $k_A(\Delta)$  and  $\gamma_A(\Delta)$  functions defined just as in Eq. (28) but using the total adiabatic radiative scattering cross section  $\sigma_\omega(\Sigma) + 2\sigma_\omega(\Pi)$ , instead of  $\sigma_\omega(j)$ ,

$$k_A(\Delta) = \frac{2\Delta^2}{\hbar^2\Omega^2} \langle [\sigma_\omega(\Sigma) + 2\sigma_\omega(\Pi)]v \rangle. \quad (29)$$

The basic expression  $J(\Delta)$  of the UFC theory and the UFC absorption profile, respectively given by Eqs. 2.48 and 2.39 of Szudy and Baylis,<sup>46</sup> are

$$J(\Delta) = \hbar^2 k_A(\Delta)/\Delta^2, \quad (30)$$

$$I(\omega) = \frac{1}{\pi} \frac{\gamma_n + \gamma_A(\Delta)}{(\omega - \omega_0 - \delta)^2 + [\gamma_n + \gamma_A(0)]^2}. \quad (31)$$

The generalization of the adiabatic UFC theory to include inelastic scattering, or nonadiabatic, effects simply requires replacing the  $\gamma_A$  quantities in Eq. (31) by the corresponding  $\gamma_E$  quantities from Eq. (23).<sup>43</sup> The resulting expression is equivalent to Eq. (25) for detunings within the impact limit if the constant  $\gamma_E(0)$  impact-limit value is used in the numerator. However, the actual  $\Delta$  dependence of  $\gamma_E(\Delta)$  in the numerator for such detunings gives rise to the Lorentzian asymmetry which has been observed experimentally for several systems<sup>47-49</sup> and has been predicted theoretically.<sup>46,50</sup> Our Eq. (23) gives a practical way of calculating the asymmetry.

#### E. Polarization ratios and depolarization rates for $^1S \rightarrow ^1P$ transitions

The numerical solution of the close-coupling equations gives the radiative scattering cross sections  $\sigma_\omega(m, q)$  for calculating the measured polarization ratios for either linear ( $q=0$ ) or circular ( $q=\pm 1$ ) polarization experiments. Recall that the quantization axis is chosen along  $\hat{e}_0$  for the former and along the Poynting vector for the latter. The following symmetry relations follow from Eq. (14) for  $j=1$ :

$$\sigma_\omega(1, 0) = \sigma_\omega(-1, 0), \quad (32a)$$

$$\sigma_\omega(1, \pm 1) = \sigma_\omega(-1, \mp 1), \quad (32b)$$

$$\sigma_\omega(\pm 1, 0) = \sigma_\omega(0, \pm 1). \quad (32c)$$

These relations and the sum rule Eq. (20) permit  $\sigma_\omega(m, q)$  to be found for all nine combinations of  $m$  and  $q$  from the three cross sections  $\sigma_\omega(0, 0)$ ,  $\sigma_\omega(1, 0)$ , and  $\sigma_\omega(1, -1)$ . The radiative excitation rate coefficients are calculated from these cross sections,

$$k_\omega(m, q) = \langle \sigma_\omega(m, q)v \rangle. \quad (33)$$

The distribution of  $m$  states produced by the radiative excitation is usually described by the irreducible spherical tensor multipole moments  $\rho^{(n)}$  of the density matrix. The  $n=2$  multipole is characterized by the alignment parameter,<sup>13,34</sup>

$$A_0(q) = \frac{k_\omega(1, q) - k_\omega(0, q)}{k_\omega}. \quad (34)$$

It is simple to show  $A_0(\pm 1) = -A_0(0)/2$  for a  $j=1$  system. The  $n=1$  multipole is characterized by the orientation parameter<sup>13,34</sup>

$$O_0(q) = \frac{k_\omega(1, q) - k_\omega(-1, q)}{\sqrt{2}k_\omega}. \quad (35)$$

The orientation parameter vanishes for  $q=0$ , and  $O_0(-1) = -O_0(1)$ . The laboratories measuring the Group-II rare-gas redistribution did not explicitly report these parameters, but chose to present their data extrapolated to the limit of zero pressure in the form of the following polarization ratios:<sup>1-3</sup>

$$P_S(\Delta) = \frac{k_\omega(0, 0) - k_\omega(1, 0)}{k_\omega(0, 0) + k_\omega(1, 0)} = \frac{3A_0(0)}{A_0(0) - 2} \quad (36)$$

and<sup>4</sup>

$$P_C(\Delta) = \frac{k_\omega(1, 1) - k_\omega(-1, 1)}{k_\omega(1, 1) + k_\omega(-1, 1)} = \frac{3\sqrt{2}O_0(1)}{2 - A_0(0)}. \quad (37)$$

Actually the same six-channel close-coupling calculation which yields the  $^1P \leftarrow ^1S$  radiative  $S$ -matrix elements also gives the five independent nonradiative  $S$ -matrix elements needed to calculate the collisional depolarization cross sections for the excited  $^1P$  state in terms of the reduced Grawert partial cross sections,<sup>36,51,52</sup>

$$\sigma_c(m, m') = \sum_g (j j g | m, m')^2 \sigma_c^g, \quad (38)$$

where

$$\sigma_c^g = \frac{\pi}{k_c^2} \sum_{l,l'} \left| \sum_J (-1)^J (2J+1) W(jljl'; Jg) \times \{ \delta_{ll'} - S(ljJ, l'jJ) \} \right|^2, \quad (39)$$

and  $\hbar^2 k_c^2 / 2\mu$  is the excited-state asymptotic kinetic energy. By measuring the pressure dependence of the  $P_S$  and  $P_C$  polarization ratios, it is possible to find the collisional destruction rate coefficients  $k_c^{(2)}$  and  $k_c^{(1)}$  of alignment and orientation.<sup>2,4</sup> These multipole-destruction rate coefficients may be written in terms of the collisional depolarization rate coefficients,<sup>13</sup>

$$k_c(m, m') = \langle \sigma_c(m, m') v \rangle, \quad (40)$$

where

$$k_c^{(2)} = 3k_c(1, 0), \quad (41a)$$

$$k_c^{(1)} = k_c(1, 0) + 2k_c(-1, 1). \quad (41b)$$

Radiative scattering theory may be used to show that the following special relationships apply for detunings in the impact limit:<sup>42</sup>

$$k_c(-1, 1) = \lim_{\Delta \rightarrow 0} \frac{4\Delta^2}{\hbar^2 \Omega^2} k_\omega(-1, 1), \quad (42a)$$

$$k_c(1, 0) = \lim_{\Delta \rightarrow 0} \frac{4\Delta^2}{\hbar^2 \Omega^2} k_\omega(1, 0). \quad (42b)$$

It is simple to show from these relationships that the polarization ratios take on the following form in the impact limit:

$$P_S(\Delta=0) = \frac{1 - k_c^{(2)}/2k_E(0)}{1 - k_c^{(2)}/6k_E(0)}, \quad (43a)$$

$$P_C(\Delta=0) = \frac{1 - k_c^{(1)}/2k_E(0)}{1 - k_c^{(2)}/6k_E(0)}, \quad (43b)$$

where  $k_E(0)$  is the broadening rate coefficient of Eq. (28). These expressions are known from standard impact theory<sup>53</sup> and were used in Refs. 1 and 4 to estimate the impact-limit polarization ratios from the measured rate coefficients. Alternatively, the broadening coefficient can be found if  $k_c^{(2)}$  and  $P_S(\Delta=0)$  are known,

$$k_E(0) = k_c^{(2)} \frac{6(1 - P_S)}{3 - P_S}. \quad (44)$$

### III. MOLECULAR POTENTIALS

In order to carry out the numerical solution to the close-coupling equations, we must have the  $W_0(R)$ ,  $W_1(R)$ , and  $W_2(R)$  Born-Oppenheimer potentials for the respective  $X^1\Sigma$ ,  $A^1\Pi$ , and  $B^1\Sigma$  states. Since no meaningful data exists for these potentials from theoretical or experimental sources, we have tried a combination of *ab initio* calculations and empirical adjustment of potentials to try to get realistic approximate potentials for these

states which can account for the available data. We will assume that these potentials can be represented as a sum of a repulsive exchange-overlap term and an attractive dispersion term,

$$W_i(R) = V_{ri}(R) - V_{di}(R). \quad (45)$$

The potential is difficult to calculate accurately, since the shallow van de Waals well region is determined by the balance between large repulsive and attractive forces. Although one-electron pseudopotential and model potential methods have been fairly successful for calculating alkali-metal-rare-gas potentials,<sup>54</sup> their use is less well developed for effective two-electron systems such as alkaline-earth-metal-rare-gas molecules. The best calculation we could do for SrAr would be a large-scale configuration-interaction (CI) calculation analogous to the NaAr calculation of Saxon, Olson, and Liu.<sup>55</sup> Since such a calculation was not realistically possible for us at the time these potentials were needed, we instead have used various approximations to estimate the repulsive and attractive contributions in Eq. (45).

#### A. Repulsive potential

The Hartree-Fock  $X^1\Sigma$  ground state of SrAr was first obtained using a double- $\zeta$  plus polarization basis for Ar and a triple- $\zeta$  basis for Sr, which was found necessary to represent the excited  $^1P$  Sr atom. The Hartree-Fock orbitals were used in a restricted CI calculation which included all single and double excitations from the Sr doubly occupied  $5s\sigma$  valence orbital. This CI scheme not only excludes any dispersion-type excitations, but also neglects Sr core and Ar valence-shell excitations. The resulting potentials can be fit to an exponential form using the constants in Table IV,

$$V_{ri}(R) = A_i e^{-(B_i + C_i R)R}. \quad (46)$$

Since the Ar orbitals are frozen in their ground-state Hartree-Fock form and do not have an opportunity to relax in the field of the excited state Sr  $p$  orbital in this limited CI calculation, we might expect the calculated exchange-overlap potentials to be too repulsive, especially for the  $B^1\Sigma$  state, the most repulsive of the three. In fact, we find that the excited-state potentials must be made significantly less repulsive in order to improve agreement between the calculated and measured  $k_E(\Delta)$  and  $P_S$ .

The SrAr potentials are qualitatively similar to the corresponding nonrelativistic potentials for the alkali-metal-rare-gas molecules. The least repulsive state of the three is the  $A^1\Pi$  state, for which the Ar approach to Sr is in the nodal plane of the Sr  $5p\pi$  orbital. The most repulsive is the  $B^1\Sigma$  state, for which the Ar approach is in the direction of the maximum density of the "dumbbell" of the Sr  $5p\sigma$  orbital. Therefore, the  $A^1\Pi$  state leads to a red-shifted difference potential relative to the asymptotic difference  $\hbar\omega_0$ , whereas the  $B^1\Sigma$  state leads to a blue-shifted difference potential. This qualitative behavior should be generic for the alkaline-earth-metal-rare-gas systems, and applies to the adjusted potentials described below as well.

TABLE IV. Numerical potential fitting parameters. All parameters in atomic units: 1 a.u. (energy) =  $e^2/a_0 = 4.359\,814 \times 10^{-18}$  j, 1 a.u. (length) =  $a_0 = 0.529\,177 \times 10^{-8}$  cm.

State	$V_r$			Adjusted		
	A	Original B	C	A	B	C
$X^1\Sigma$	0.102 675	0.031 476	0.051 087	17.75	1.064	0.0
$A^1\Pi$	0.164 881	0.186 473	0.043 957	1.1095	0.8715	0.0
$B^1\Sigma$	1.755 220	0.666 304	0.0	11.09	0.921	0.0

State	$V_d$		$C_{\text{eff}} = 588.24$	$R_m = 12.003$
	D = 0.079 370	Original E = 0.499 889		
$X^1\Sigma$				

State	$C_{\text{eff}}$	$C_{\text{eff}}$
	Original	Adjusted
$X^1\Sigma$	588.24	450
$A^1\Pi$	622	500
$B^1\Sigma$	888	1200

### B. Dispersion potential

The damped-dispersion energy in the  $X^1\Sigma$  ground state was calculated using the methods developed by Koide<sup>56</sup> and Krauss and Neumann,<sup>57</sup>

$$V_d(R) = C_6\chi_6(R)/R^{-6} + C_8\chi_8(R)/R^{-8} + C_{10}\chi_{10}(R)/R^{-10}. \quad (47)$$

The damping coefficients  $\chi$  approach unity as  $R \rightarrow \infty$  and vanish as  $R \rightarrow 0$ . The damped dispersion series is convergent at all  $R$ , whereas the normal undamped series is only an asymptotic series (i.e., eventually divergent if too many terms are included). Calculating the three terms in Eq. (47) requires finding the dipole, octupole, and quadrupole polarizabilities and corresponding first-order wave functions<sup>57</sup> for the Sr and Ar atoms. Our calculated Hartree-Fock polarizabilities for Ar and  $C_6$ ,  $C_8$ , and  $C_{10}$  coefficients for Ar<sub>2</sub> agree with known values<sup>58</sup> to within 5%. Although our multiconfiguration self-consistent-field wave function for Sr includes correlating  $p^2$  and  $d^2$  configurations, it did not include split-shell valence-core excitations. The damped-dispersion contribution to each of the three terms in Eq. (47) is shown in Table V. The total ground-state damped dispersion energy can be fit to the function

$$V_d(R) = De^{-ER}, \quad R_m > R \quad (48a)$$

$$= C_{\text{eff}}R^{-6}, \quad R_m \leq R. \quad (48b)$$

The coefficient  $C_{\text{eff}}$  and match point  $R_m$  are chosen so that  $V_d$  and its first derivative are continuous at the match point. Note that  $C_{\text{eff}}$  contains contributions from  $C_8$  and  $C_{10}$  terms as well as  $C_6$ . The parameters in Eqs. (48) are shown in Table IV.

Our calculated Sr dipole polarizability,  $237a_0^3$ , is much larger than the measured value,  $186a_0^3$  (Ref. 59), since we have neglected the effect of core relaxation, which is

known to be important for an atom such as Sr.<sup>60</sup> Therefore, we adjust the calculated total ground-state dispersion energy by scaling the calculated value by the ratio of measured to calculated dipole polarizabilities,  $\frac{186}{237} = 0.77$ . The scaled value  $C_{\text{eff}} = 450$  for the ground state is used in the adjusted potentials described below.

There is currently no *ab initio* procedure available for calculating the damped-dispersion coefficients for excited states with allowed downward transitions. However, the series expansion method used by Mahan<sup>61</sup> and Proctor and Stwalley<sup>62</sup> for alkali-metal-rare-gas excited states can readily be generalized to the present case. Using the formulas given by Mahan,<sup>61</sup> we have

$$C_6(A^1\Pi) = \alpha(\langle r_s^2 \rangle + 4\langle r_p^2 \rangle / 5), \quad (49a)$$

$$C_6(B^1\Sigma) = \alpha(\langle r_s^2 \rangle + 7\langle r_p^2 \rangle / 5), \quad (49b)$$

where  $\alpha$  is the Ar polarizability and  $\langle r_s^2 \rangle$  and  $\langle r_p^2 \rangle$  are the expectation values of  $r^2$  for the Sr  $5s$  and  $5p$  atomic orbitals. If we use the Coulomb-approximation result<sup>61</sup> for the expectation values, respectively 15.5 and  $40a_0^2$  for

TABLE V. Calculated  $X^1\Sigma$  damped-dispersion energy in  $10^{-6}$  atomic units.

R	$R^{-6}$ term	$R^{-8}$ term	$R^{-10}$ term	Total
8	813	550	92	1455
9	526	327	56	909
10	330	187	31	548
11	206	104	18	328
12	129	58	10	197
13	82	32	4	118
14	54	18	2	74
15	36	11	1	48

the  $5s$  and  $5p$  orbitals, we find  $C_6(\pi)=530$  and  $C_6(\Sigma)=790$  in atomic units ( $e^2a_0^5$ ). When the same approximation is applied to the SrAr ground state using our calculated Ar polarizability, we find  $C_6(X^1\Sigma)=322$ , which compares well with the scaled *ab initio* value, 314 atomic units.

Since the role of damping in the excited state is unknown, the excited-state dispersion energy was fit with the same functional form as the ground state, Eq. (48). The excited-state fits were scaled from the ground-state fit in Table IV by multiplying at each  $R$  by the ratio  $C_{\text{eff}}(A^1\Pi, B^1\Sigma)/C_{\text{eff}}(X^1\Sigma)$ . The original excited-state  $C_{\text{eff}}$  values shown in Table IV which we used in the preliminary calculation we reported<sup>12</sup> were found from Eqs. (49) using the Dirac-Fock expectation value for  $\langle r_s^2 \rangle$ .<sup>63</sup>

Note that the  $B^1\Sigma$  state has the larger dispersion coefficient of the two excited states. However, the alkali-earth-metal-rare-gas  $\Sigma$  and  $\Pi$   $C_6$  coefficients do not have the 7:4 ratio of alkali-metal-rare-gas coefficients because of the extra  $5s$  valence electron. The dispersion contribution to the difference potential is red shifted for both excited states.

### C. Adjusted potentials

Our initial set of potentials were used to calculate the wing absorption spectrum, the impact broadening coefficient, the  $P_S$  polarization ratio, and the depolarization cross sections.<sup>12</sup> Since significant disagreements between calculated and measured results were found [blue wing  $k_E(\Delta)$  factor of 6 too high; red wing  $P_S$  ratio 50% too high], we conclude that the original set of potentials need to be corrected. This is not at all surprising, given the variety of approximations which had to be introduced in order to estimate the potentials. Since the potentials in the shallow van der Waals well region of  $R$  are determined by the cancellation of large positive and negative terms, they are sensitive to the approximations used. Accurate calculation of such shallow wells strains the limits of current *ab initio* methods. We did not use a systematic method such as least-squares fitting to get improved potentials, but through a trial-and-error procedure were able to obtain potentials which give much better overall agreement between theory and experiment. Although the resulting potentials still have some deficiencies, there is no simple way of assessing their inaccuracies.

The potential parameters of the adjusted potentials are shown in Table IV. The adjusted  $C_{\text{eff}}$  values for the three potentials in Table IV were used to scale the Eq. (48) fit to the calculated ground-state damped dispersion. We found that the repulsive potential  $V_r$  had to be decreased significantly for both of the excited-states. Some possible reasons for this are discussed in Sec. III A above. Although the ground-state  $V_r$  parameters are numerically different, the fits are substantially the same in both cases over the  $R$  range of importance. Since an increase in dispersion energy can mimic to some extent a decrease in exchange-repulsion energy and vice versa, we suggest that the adjusted parameters in Table IV be viewed solely as numerical fitting parameters and, with the possible exception of the ground state, not be individually interpreted

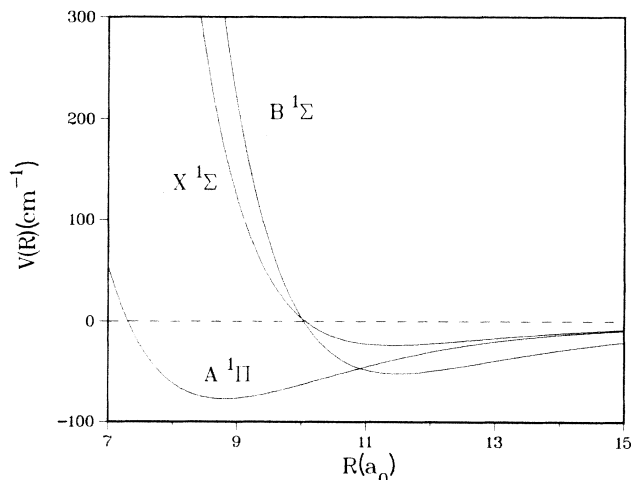


FIG. 1. Adjusted Born-Oppenheimer potential energy curves  $W(R)$  for the  $X^1\Sigma$ ,  $A^1\Pi$ , and  $B^1\Sigma$  states of Sr + Ar. All curves are referred to the same asymptote,  $W(\infty)=0$ .

physically as uncorrelated parameters.

The adjusted potentials are shown in Fig. 1. The biggest change is in the  $B^1\Sigma$  potential, for which the respective  $D_e, R_e$  values changed from  $4 \text{ cm}^{-1}$  at  $17a_0$  to  $52 \text{ cm}^{-1}$  at  $11.5a_0$ . This dramatic change was necessary to account for the blue-wing absorption data and the existence of a red satellite feature, as well as the polarization data. The  $D_e, R_e$  change in the  $A^1\Pi$  potential from  $57 \text{ cm}^{-1}$  at  $10.3a_0$  to  $80 \text{ cm}^{-1}$  at  $8.8a_0$  is relatively much less than for the  $B^1\Sigma$  potential. The most accurate potential is expected to be that for the ground state, which has a shallow van der Waals well about  $24 \text{ cm}^{-1}$  deep with an  $R_e$  near  $11.5a_0$ . Since the  $A^1\Pi-X^1\Sigma$  difference potential is red shifted for both the  $V_r$  and  $V_d$  contributions, the  $A^1\Pi$  state gives rise to a quasistatic red wing and anti-static blue wing of the spectral profile. However, the  $B^1\Sigma-X^1\Sigma$  difference potential is red shifted at large  $R$  due to the dispersion component but blue shifted at small

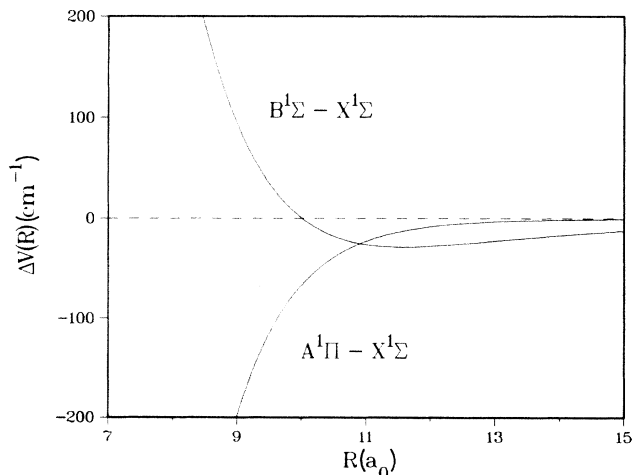


FIG. 2. Calculated  $A^1\Pi-X^1\Sigma$  and  $B^1\Sigma-X^1\Sigma$  difference potentials for the adjusted potentials.

$R$  due to the repulsive component, so that there is necessarily an extremum on the red side of the difference potential. Therefore, the  $B^1\Sigma$  state has a quasistatic blue wing and a red satellite feature which may or may not be prominent depending on the details of the difference potential. These generic features of the SrAr difference potentials should be true for all Group-IIa—rare-gas  $nsnp^1P$ — $ns^2^1S$  transitions. The SrAr difference potentials are shown in Fig. 2.

#### IV. CALCULATED RESULTS

The calculations were carried out using our standard close-coupling scattering code<sup>28,36</sup> based on the Gordon algorithm.<sup>64</sup> Solution of the set of six coupled equations for a single total angular momentum  $J_0$ , incident energy  $\epsilon_0$ , and detuning  $\Delta$  required about 1.5 sec on a CYBER 205 computer. Calculations were done for a range of detunings for a collision energy of  $500\text{ cm}^{-1}$ , which corresponds to  $kT$  for  $T=719\text{ K}$ . The energy variation and thermal averaging of  $k_E(\Delta)$  was studied at selected detunings of  $\pm 100\text{ cm}^{-1}$ ,  $-30\text{ cm}^{-1}$ ,  $20\text{ cm}^{-1}$ ,  $\pm 0.5\text{ cm}^{-1}$ , and  $0.01\text{ cm}^{-1}$ .

##### A. Reduced radiative $s_\omega$ matrix elements

The choice of radiation flux  $\phi$  as a scaling parameter is arbitrary within wide limits. The flux should neither be too small, to avoid numerical differencing problems, nor too large, to avoid nonlinear strong-field saturation effects. Quite satisfactory results were obtained by choosing  $\phi$  so that the  $s_\omega$  typically had magnitudes on the order of  $10^{-5}$ – $10^{-6}$ . A flux  $\phi=0.01\text{ W cm}^{-2}$  was used except for very small detunings in the impact limit, where the flux was adjusted downwards to keep the magnitudes of  $s_\omega$  small and satisfy  $\hbar\Omega \ll \Delta$ . In any case the calculated  $s_\omega$  were found to be perfectly linear in  $\phi^{1/2}$  over many decades of variation of  $\phi$ . Some specific numerical examples may be found in Table II of Ref. 39.

Some care must be taken in the case of optical collisions in order to extract the desired field-free Hund's case-( $e$ )  $s_\omega$  matrix elements. Our scattering code obtains the asymptotic  $S$  matrix in the representation found by diagonalizing the asymptotic electronic-rotational-radiation coupling potential matrix, that is, in an asymptotic dressed-state basis. This poses a problem when we set up the radiative close coupling with a single set of six coupled equations in which all three branches are treated simultaneously. Since there are three degenerate  $j=1$  final channels (one for each branch) with the same final  $l=l_0$  that are mixed by radiative couplings to the initial  $j=0$ ,  $l_0=J_0$  channel, any  $S$  matrix calculated in an asymptotically diagonal dressed representation is susceptible to numerically ambiguous rotations of basis. Thus,  $S$  should always be rotated back to the unambiguous case-( $e$ ) representation taking care to use the explicit orthogonal transformation which actually diagonalized the asymptotic basis and defined the close-coupled  $S$ . This procedure is discussed in more detail in the Appendix of Ref. 13.

The coupled equations can be set up in an equivalent al-

ternative fashion as three separate sets of coupled equations, one for each of the three possible branches. Such a calculation can be done for Sr + Ar by setting up for each  $J_0$  one set of three-coupled equations for the  $P$  branch (i.e., for the initial channel and the two final channels), a similar set for the  $R$  branch, and a set of two coupled equations for the  $Q$  branch. Since the asymptotically degenerate  $j=1$  channels for the  $P$  and  $R$  branches have different  $l$  values, the numerical diagonalization at large but finite  $R$  projects the correct case-( $e$ ) basis functions. Since there is only a single final channel with the same  $l$  as the initial channel,<sup>13</sup> there is no asymptotic radiative mixing of final channels. The extraction of the numerical  $s_\omega$  from the asymptotic solutions is therefore straightforward and unambiguous.

Both calculations, that with each branch calculated separately and that with all three calculated simultaneously, were tested for Sr + Ar and found to yield identical results. The approximate  $N^3$  scaling of computation time, where  $N$  is the number of channels, shows that the separate branch calculation will generally be more computationally efficient than the full calculation (e.g., compare  $6^3$  versus  $2 \times 3^3 + 2^3$ ). However, the advantages of the full six-channel formulation in computational logistics for the Sr + Ar problem was judged to outweigh the time-savings advantage of the separate branch calculation. Certainly the separate branch calculation is likely to be preferred for more complex systems with more channels.

##### B. Opacity functions

Any cross section can be written in terms of an opacity function  $P(J)$  defined by

$$\sigma = \frac{\pi}{k^2} \sum_J (2J+1)P(J). \quad (50)$$

The opacity was calculated for the necessary range of  $J$  for each of the various partial cross sections needed, that is, the transfer cross sections  $\sigma'_{\omega}$ , the branch cross sections  $\sigma_{\omega}^b$ , the polarization cross sections  $\sigma_{\omega}(mq)$ , and the Grawert cross sections  $\sigma_{\omega}^g$ . Although  $P(J)$  is typically required for several hundred  $J$  values,  $P(J)$  in many cases was sufficiently smoothly varying with  $J$  that interpolation using only every  $n$ th value of  $J$  was successful ( $n=2, 3, 4, \text{ or } 5$ ). Extrapolation of the opacity function beyond some large  $J$  cutoff  $J_{\max}$  was done by fitting the last two calculated opacities to the form  $AJ^{-a}$ . The overall numerical accuracy of the calculated partial cross sections for the given set of potentials is expected to be in the range 0.1–1%.

There are three quite distinct regions of detuning for which the behavior of the cross sections is characteristically different. These regions are the far wings, the intermediate wings, and the impact region, associated with approximate detuning ranges of  $|\Delta| > 50\text{ cm}^{-1}$ ,  $50\text{ cm}^{-1} > |\Delta| > 2\text{ cm}^{-1}$ , and  $|\Delta| < 2\text{ cm}^{-1}$ , respectively. The suggested boundaries of these regions are by no means precise and are meant only to give a rough indication of where characteristic changes occur.

In the far-wing detuning region, absorption is predominantly to a single molecular state, to the  $A^1\Pi$  state for

red detuning and to the  $B^1\Sigma$  state for blue detuning. The classical Franck-Condon principle applies and quasistatic theory<sup>65,28</sup> is a good approximation for the total absorption coefficient. Kulander and Rebrost<sup>30</sup> have demonstrated the equivalence between quasistatic theory and the Landau-Zener curve-crossing model for radiative scattering. The normalized absorption coefficient for a collision energy  $\epsilon_0$  is

$$K_\omega = \sigma_\omega v / \phi = \frac{32\pi^4}{3\lambda} \frac{(R^* \mu^*)^2}{d\Delta V^*} (1 - V^*/\epsilon_0)^{1/2}, \quad (51)$$

where the asterisk implies that the quantities are evaluated at the internuclear separation  $R^*$  where  $\hbar\omega$  equals the difference potential;  $V^*$  is the ground-state potential at  $R=R^*$ . The thermally averaged absorption coefficient is given by Eq. (51) with the square-root factor replaced by the Boltzmann factor  $e^{-V^*/k_B T}$

The branch partial cross sections  $\sigma_\omega^b$ , Eq. (19), for far-wing detuning are found to follow closely the ratio of Hönl-London line strength factors<sup>66</sup> for the appropriate transitions. These ratios  $\sigma_\omega^P:\sigma_\omega^Q:\sigma_\omega^R:\sigma_\omega$  are  $\frac{1}{2}:0:\frac{1}{2}:1$  for a  $^1\Sigma\text{-}^1\Sigma$  transition and  $\frac{1}{2}:1:\frac{1}{2}:2$  for a  $^1\Pi\text{-}^1\Sigma$  transition. These ratios were found to hold to within a few percent for red and blue far-wing detuning. Figure 3(a) shows the opacity functions for the  $P$ ,  $Q$ , and  $R$  partial cross sections for a red detuning of  $-100\text{ cm}^{-1}$ , a collision energy of  $500\text{ cm}^{-1}$ , and a radiation flux of  $0.01\text{ W cm}^{-1}$ . Although these opacities oscillate with  $J$  in a similar fashion due to nearly common Franck-Condon factors, they oscillate with  $J$  slightly out of phase with each other due to the different final  $J$ 's. The calculated partial-cross-section ratios for this example are  $0.48:1.00:0.52:2.00$ . Figure 3(b) shows for the same case the opacities for  $\sigma_\omega(m=0)$  and  $\sigma_\omega(m=1)$  for  $q=0$ . The fact that these

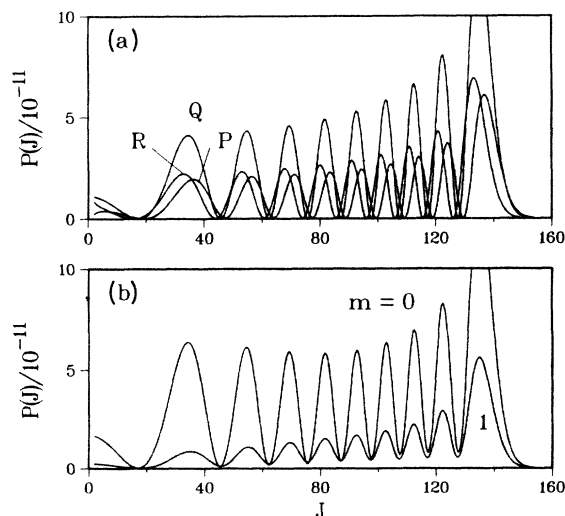


FIG. 3. Far-red-wing opacity functions  $P(J)$  for a collision energy of  $\epsilon_0=500\text{ cm}^{-1}$ , detuning of  $\Delta=-100\text{ cm}^{-1}$ , and  $\phi=0.01\text{ W cm}^{-2}$ . (a) Opacities for the  $P$ -,  $Q$ -, and  $R$ -branch partial cross sections. (b) Opacities for the  $\sigma_\omega(0,0)$  (upper curve) and  $\sigma_\omega(1,0)$  (lower curve) cross sections.

oscillate nearly in phase with each other is due to the common Franck-Condon excitation through the  $A^1\Pi$  state for both.

A totally different behavior applies for small detunings, where the well-known impact approximation is valid. The detuning must be sufficiently small that  $\Delta/\hbar \ll \tau_c^{-1}$ , where  $\tau_c$  is the duration of the collision. Close-coupling effects are dominant in this region, and a purely adiabatic description in terms of isolated  $^1\Sigma$  and  $^1\Pi$  molecular states is inappropriate. Both states contribute to the absorption, and their nonadiabatic mixing cannot be neglected. Special relations exist in the impact limit between radiative and nonradiative scattering, and exact relations such as Eqs. (42) and (43) apply. Figure 4(a) shows the opacities at a detuning of  $1\text{ cm}^{-1}$  for the total cross section and the  $Q$  branch, and Fig. 4(b) shows the opacity functions for  $\sigma_\omega(m=0)$  and  $\sigma_\omega(m=1)$  for  $q=0$ . These latter functions do not look at all like each other, in contrast to the far-wing behavior of Fig. 3(b). The  $m=1$  opacity function is found to be proportional to that for  $\sigma_c(1,0)$ , as predicted by Eq. (42b), but it does not follow the oscillations of the  $Q$ -branch opacity.

The intermediate detuning range between the far wings and the impact limit has some common features of both. Both molecular states contribute to the absorption, which may be influenced by nonadiabatic mixing of states. However, the excitation Franck-Condon factors no longer are determined by the asymptotic properties of the nonradiative scattering wave function as in the impact limit. For our problem both the  $A^1\Pi$  quasistatic wing and a  $B^1\Sigma$  satellite feature contribute to the intermediate red-wing absorption, whereas the intermediate blue wing has contributions from the  $B^1\Sigma$  quasistatic wing and the  $A^1\Pi$  antistatic wing. The opacity functions for  $\sigma_\omega(m=0)$  and  $\sigma_\omega(m=1)$  in Fig. 5(b) for intermediate blue detuning of  $20\text{ cm}^{-1}$  shows a characteristic complexity due to contributions from both types of absorption. There are no simple regularities to be found, as in the im-

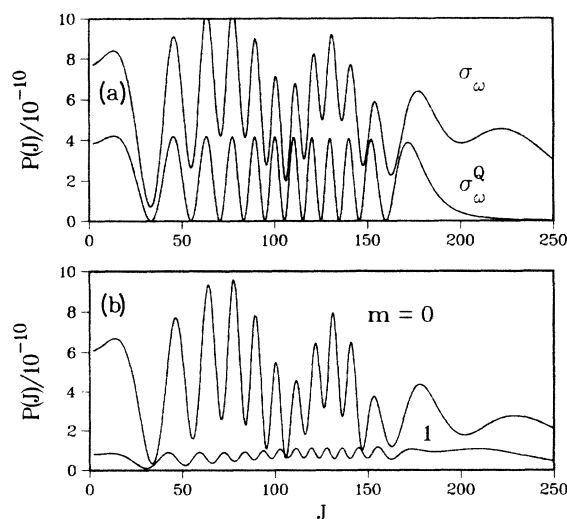


FIG. 4. Impact-limit opacity functions for  $\epsilon_0=500\text{ cm}^{-1}$ ,  $\Delta=1\text{ cm}^{-1}$ , and  $\phi=0.0001\text{ W cm}^{-2}$ . (a) For total cross section  $\sigma_\omega$  and  $Q$  branch. (b) As in Fig. 3(b).

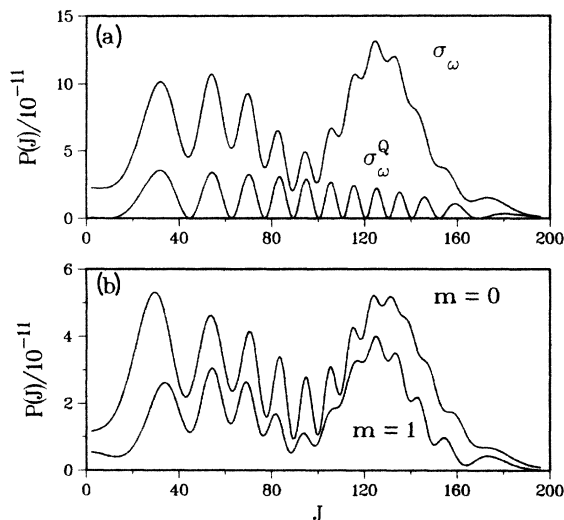


FIG. 5. Intermediate-wing opacity functions for  $\epsilon_0=500$   $\text{cm}^{-1}$ ,  $\Delta=20$   $\text{cm}^{-1}$ , and  $\phi=0.01$   $\text{W cm}^{-2}$ . (a) As in Fig. 4(a). (b) As in Figs. 3(b) and 4(b).

compact limit and far wings, and the radiative scattering amplitudes are given by a coherent sum of interfering contributions from  $^1\Sigma$  and  $^1\Pi$  absorption.

Since a  $^1\Sigma\text{-}^1\Sigma$  transition has no  $Q$  branch, the  $\sigma_\omega^Q$  partial cross section represents absorption to the  $^1\Pi$  state only. This is true for any detuning, including the impact limit. In fact, if the Hönl-London ratios are assumed for the  $P$ ,  $Q$ , and  $R$  contributions of the Szudy-Baylis adiabatic Franck-Condon theory, then  $2\sigma_\omega^Q$  from our close-coupling calculation is just the quantity needed to predict the absorption coefficient for the  $^1\Pi\text{-}^1\Sigma$  transition. The difference  $\sigma_\omega - 2\sigma_\omega^Q$  gives an estimate of the contribution of the  $^1\Sigma\text{-}^1\Sigma$  transition to the total. Therefore, the  $Q$ -branch opacities in Fig. 5(a) can be used to estimate the contribution of the  $A$   $^1\Pi$  absorption to the total. For the example in Fig. 5,  $2\sigma_\omega^Q$  represents 36% of the total cross section.

### C. Frequency-dependent broadening coefficient

Figure 6 shows the frequency-dependent broadening coefficient  $k_E(\Delta)$  of Eq. (28) for a collision energy of  $500$   $\text{cm}^{-1}$ , as well as several thermally averaged points. This quantity is independent of the value of the radiation flux  $\phi$  actually used to do the calculation at the various detunings, as discussed in Secs. II B and IV A above. The coefficient  $k_E(\Delta)$  is not very sensitive to  $T$  for the range of detunings shown, since the van der Waals wells are shallow compared to  $kT$ . An estimate of the contribution of the  $A$   $^1\Pi$  state to the absorption is given by the function defined by

$$k_E^\Pi(\Delta) = 2k_E^Q(\Delta). \quad (52a)$$

Similarly the contribution of the  $B$   $^1\Sigma$  state can be estimated from the following function defined by the close-coupling calculation:

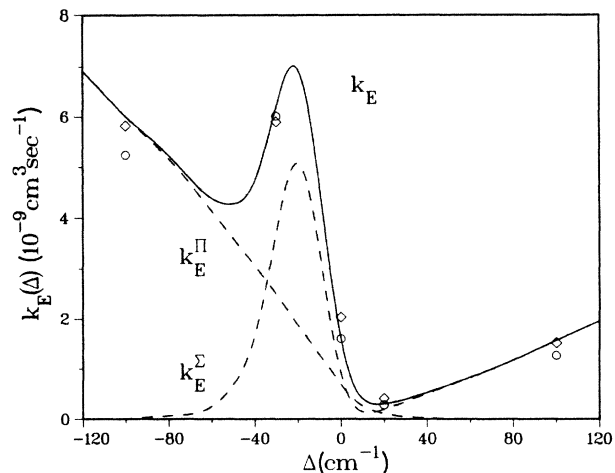


FIG. 6. Calculated frequency-dependent broadening coefficient  $k_E(\Delta)$  for a collision energy of  $\epsilon_0=500$   $\text{cm}^{-1}$  (line). The points show thermally averaged values for  $T=500$  K ( $\circ$ ) and  $1000$  K ( $\diamond$ ). The dashed lines show the estimated contributions from  $A$   $^1\Pi$  and  $B$   $^1\Sigma$  absorption, as defined by Eq. (52).

$$k_E^\Sigma(\Delta) = k_E(\Delta) - k_E^\Pi(\Delta). \quad (52b)$$

These two functions are also shown in Fig. 6. The far red- and blue-wing absorption are dominated by, respectively,  $A$   $^1\Pi$  and  $B$   $^1\Sigma$  absorption, as expected. There is prominent satellite feature peaking near  $\Delta = -20$   $\text{cm}^{-1}$  associated with the extremum in the  $B$ - $X$  difference potential at  $\Delta = -28$   $\text{cm}^{-1}$  (see Fig. 2).

The calculated  $k_E(\Delta)$  function for  $\epsilon_0=500$   $\text{cm}^{-1}$  is compared to the available experimental data in Fig. 7, which shows the red- and blue-wing absorption data of Harima *et al.*<sup>67</sup> and the experimental impact-limit results.<sup>68,69</sup> Equations (27) and (28) were used to convert the wing data to the form required by the figure. The overall comparison between theory and experiment is favorable, although there are significant differences of de-

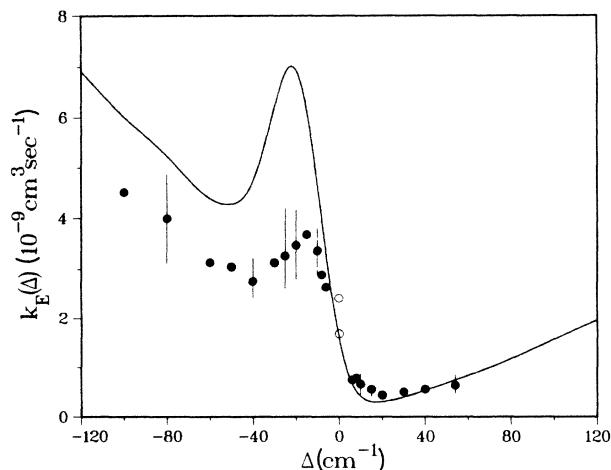


FIG. 7. Comparison of the calculated  $k_E(\Delta)$  for  $\epsilon_0=500$   $\text{cm}^{-1}$  and the wing ( $\bullet$ ) and impact-limit ( $\circ$ ) data.

tail. The most obvious difference is in the magnitude of the  $B^1\Sigma$  satellite feature. Our potentials predict this feature to be too large relative to the data. However, the calculated and measured far-wing data are in fairly reasonable agreement. The far-wing data of Harima *et al.*<sup>67</sup> may not be reliable, since the absorption data of Alford *et al.*<sup>3</sup> for the closely related system Ba + Ar shows large disagreements with that of Harima *et al.*<sup>67</sup> for detunings in excess of about  $50 \text{ cm}^{-1}$ .

Our calculated Lorentzian half width at half maximum (HWHM) pressure-broadening coefficient for the impact-limit core is  $k_E(0) = 1.8 \times 10^{-9} \text{ cm}^3 \text{ sec}^{-1}$  at 700 K. The calculated values vary between  $1.6 \times 10^{-9}$  and  $2.0 \times 10^{-9} \text{ cm}^3 \text{ sec}^{-1}$  for  $T$  between 500 and 1000 K. The calculation compares well with the experimental broadening coefficients which have been reported,  $(2.4 \pm 0.06) \times 10^{-9} \text{ cm}^3 \text{ sec}^{-1}$  at 700 K (Ref. 68) and  $1.68 \times 10^{-9} \text{ cm}^3 \text{ sec}^{-1}$  at 750 K.<sup>69</sup> If an impact-limit value of  $P_S = 0.65 \pm 0.03$  is estimated by extrapolating the data of Alford *et al.*<sup>2</sup> using the shape of the calculated  $P_S$ -versus- $\Delta$  curve (see Fig. 8), then Eq. (44) predicts  $k_E(0) = (1.8 \pm 0.3) \times 10^{-9} \text{ cm}^3 \text{ sec}^{-1}$  near 800 K, given that  $k_c^{(2)} = (1.58 \pm 0.19) \times 10^9 \text{ cm}^3 \text{ sec}^{-1}$ .<sup>2</sup> Thus the polarization data of Alford *et al.*<sup>2</sup> seem more consistent with the broadening coefficient of Ref. 69 than that of Ref. 68.

The variation of  $k_E(\Delta)$  across the impact-limit region near  $\Delta = 0$  gives rise to a dispersion component in the absorption profile. If we define a slope parameter as in Ref. 48,

$$k_E(\Delta) = k_E(0)(1 - b\Delta), \quad (53)$$

our calculations predict  $b = 0.14 \text{ (cm}^{-1}\text{)}^{-1}$  for  $T = 700 \text{ K}$ . Since  $b$  is proportional to collision duration, it decreases as  $T$  increases due to averaging over more rapid collisions. Our calculated values vary from 0.16 to 0.11  $\text{(cm}^{-1}\text{)}^{-1}$  as  $T$  ranges from 500 to 1000 K. Although the asymmetry

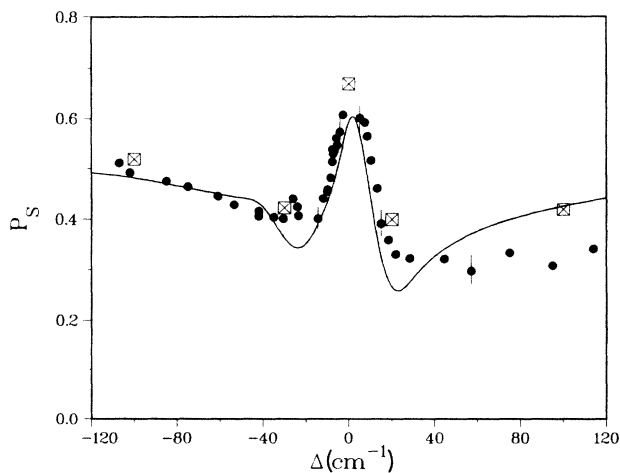


FIG. 8. Calculated polarization ratio  $P_S$  for a collision energy  $\epsilon_0 = 500 \text{ cm}^{-1}$  (line). The squares ( $\boxtimes$ ) show the thermally averaged values for  $T = 800 \text{ K}$  at selected detunings. The solid circles ( $\bullet$ ) show the experimental data.

parameter has not been measured for Sr + Ar, our results are comparable in magnitude to the multiplet average value,  $0.18 \text{ (cm}^{-1}\text{)}^{-1}$  measured by Walkup *et al.*<sup>48</sup> for room temperature for the  $^2P^2S$  transition in the analogous system Na + Ar.

#### D. Linear-polarization ratios

Figure 8 shows the results of our calculation of the polarization ratio  $P_S$  and comparison with the experimental data of Alford *et al.*<sup>2</sup> The figure shows our calculation for  $\epsilon_0 = 500 \text{ cm}^{-1}$  and several thermally averaged points at  $T = 800 \text{ K}$ . The overall agreement is good. The thermally averaged theoretical points appear to agree with the measured points within the experimental uncertainty, except for far-blue-wing detuning. This disagreement seems consistent with the known deficiency of the  $B^1\Sigma$  potential, which fails to reproduce the red-wing satellite feature in the absorption data. If the experimental data are extrapolated into the impact region according to the calculated shape of the  $\epsilon_0 = 500 \text{ cm}^{-1}$  curve, the impact-limit value  $P_S = 0.65$  discussed in Sec. IV C above results. This extrapolated value agrees well with the calculated impact-limit value 0.67.

Although thermal averaging is needed for accurate comparison to data, the curve for fixed collision energy in Fig. 8 shows the basic qualitative features of the detuning dependence. The main effect of thermal averaging is to fill in the "dip" regions for intermediate detunings near  $\Delta = \pm 20 \text{ cm}^{-1}$ . Figure 9 shows the temperature dependence of  $P_S$  for selected detunings. Since the predicted temperature variation over a range of temperature which would be experimentally accessible is comparable to the range of error bars for the Alford *et al.*<sup>2</sup> experiment, it would be difficult to measure any significant or interesting  $T$  dependence in  $P_S$  in such an experiment.

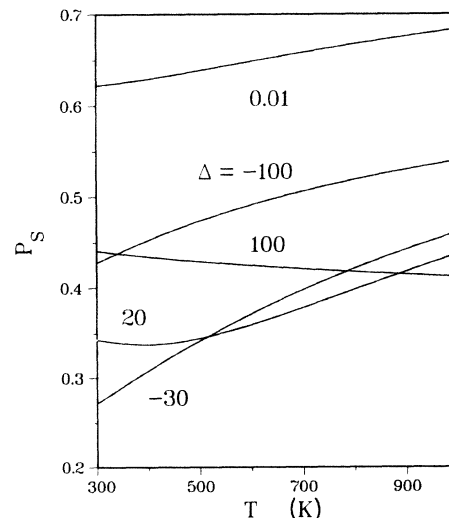


FIG. 9. Calculated temperature dependence of the  $P_S$  polarization ratio for selected detunings.

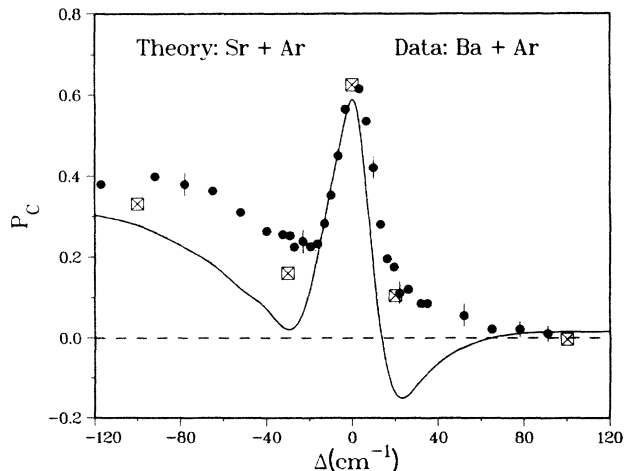


FIG. 10. Calculated Sr + Ar polarization ratio  $P_C$  for a collision energy  $\epsilon_0=500 \text{ cm}^{-1}$  (line) and thermally averaged points for  $T=900 \text{ K}$  ( $\boxtimes$ ). The experimental data for Ba + Ar is also shown ( $\bullet$ ).

### E. Circular-polarization ratios

Figure 10 shows our calculated results for  $P_C$  for a fixed collision energy  $\epsilon_0=500 \text{ cm}^{-1}$  as well as several thermally averaged points at 900 K. Although there are no  $P_C$  data for Sr + Ar, Alford *et al.*<sup>4</sup> have made measurements for the similar system Ba + Ar. Both the total-wing absorption coefficients and linear-polarization ratios for Sr + Ar<sup>67,2</sup> and Ba + Ar (Refs. 70 and 3) are known from experiment to be very similar. Therefore, we also show the  $P_C$  data for Ba + Ar in Fig. 10. The good qualitative comparison evident for the thermally averaged Sr + Ar calculation and the Ba + Ar measurements gives credence to the belief that the two systems should have very similar  $P_C$  ratios.

Thermal averaging is important for  $P_C$  in comparing theory and experiment just as it was for  $P_S$ . Figure 11

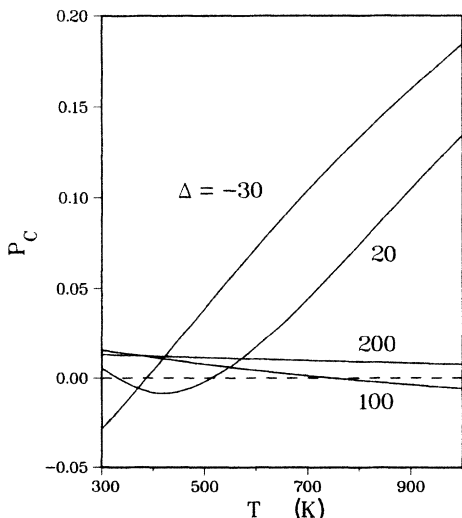


FIG. 11. Calculated temperature dependence of the  $P_C$  polarization ratio for Sr + Ar at selected detunings.

shows the  $T$ -dependent  $P_C$  ratios for several detunings. There is a strong temperature dependence in the intermediate wing  $P_C$  ratios, which may actually change sign as a function of  $T$ . As a general rule, the  $P_S$  and  $P_C$  ratios for intermediate-wing detuning tend to be more sensitive to details of the potentials than the ratios for impact or far-wing detunings. Part of the reason for this sensitivity is the varying contributions from the  $\Sigma$  and  $\Pi$  absorption (static, antistatic, and satellite) in this detuning range. These calculations are suggestive of the magnitude of possible observable effects, but should not be taken too seriously until definitive potentials become available.

One perhaps surprising feature predicted by our calculations and confirmed by the data is the persistence at large blue detuning of a small but nonvanishing  $P_C$ . Theoretical considerations show that excitation of a pure  $^1\Sigma$  state should lead to  $P_C=0$ .<sup>4</sup> However, the Coriolis mixing of the excited  $B^1\Sigma$  and  $A^1\Pi$  states causes some  $\Pi$  character to be acquired by the  $^1\Sigma$  state so that a finite  $P_C$  results.

### F. Collisional rate coefficients $k_C$

The cross sections for elastic and depolarizing collisions of Sr  $^1P_1$  + Ar are shown in Fig. 12 in the form of excited-state collision energy-dependent rate coefficients,  $k_C=\sigma_C v$ . The corresponding thermally averaged quantities are given in Table VI. The calculated value for the alignment destruction rate coefficient,  $k_C^{(2)}=1.6\times 10^{-9} \text{ cm}^3 \text{ sec}^{-1}$  in the  $T=700\text{--}900 \text{ K}$  range is in excellent agreement with the measured value,  $(1.58\pm 0.19)\times 10^{-9} \text{ cm}^3 \text{ sec}^{-1}$ .

Although there is no measurement of the orientation destruction rate coefficient  $k_C^{(1)}$  for Si + Ar, there is a measurement for both  $k_C^{(1)}$  and  $k_C^{(2)}$  for the closely related Ba + Ar system, for which the ratio  $k_C^{(1)}/k_C^{(2)}=1.12\pm 0.10$ .<sup>4</sup> We find a similar ratio, 1.10 at 900 K, for Sr + Ar, as seen from Table VI. In order to explain a ratio of this magnitude using the theory for pure dispersion potentials ( $-C_6/R^{-6}$ ), Alford *et al.*<sup>4</sup> found that they had to assume a ratio  $C_6(^1\Sigma)/C_6(^1\Pi)=4$ . This ratio is signi-

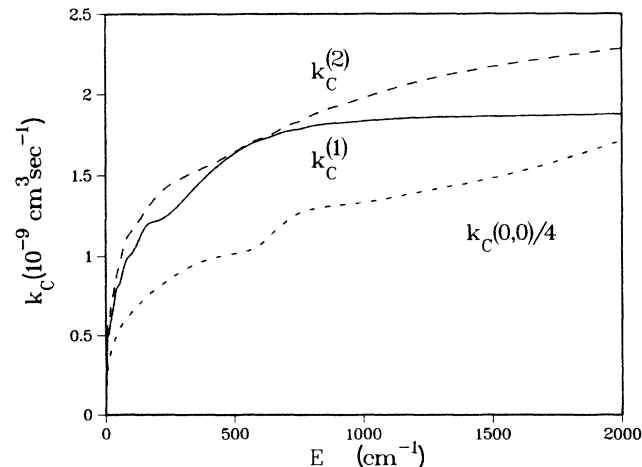


FIG. 12. Calculated energy-dependent rate coefficients,  $k_C=\sigma_C v$ , for Sr  $^1P_1$  + Ar elastic and depolarizing collisions.

TABLE VI.  $^1P_1$  collisional rate coefficients in  $10^{-9}$   $\text{cm}^3\text{sec}^{-1}$ .

$T$ (K)	$k_C(0,0)$	$k_C(1,1)$	$k_C^{(1)}$	$k_C^{(2)}$	$k_C^{(1)}/k_C^{(2)}$
500	4.00	3.95	1.57	1.47	1.07
600	4.25	4.19	1.65	1.53	1.08
700	4.47	4.41	1.71	1.58	1.09
800	4.69	4.61	1.76	1.61	1.09
900	4.89	4.80	1.81	1.64	1.10
1000	5.08	4.98	1.86	1.67	1.11

ificantly different from the ratio 2.4 of  $C_{\text{eff}}$  coefficients (see Table V) used in our calculations. We would advise some caution in using pure dispersion potentials for interpreting depolarization rates, especially since such theories, which do not account for short-range forces, were recently found to be quantitatively rather poor when compared to measured alignment destruction rates for Sr  $^3P_1$  (Ref. 71) and Yb  $^3P_1$  (Ref. 72) + rare gases.

Since the calculated elastic scattering cross sections for the  $m=0$  and 1 Zeeman sublevels of  $^1P_1$  are nearly the same, only the coefficient for  $m=0$  is shown in Fig. 12; the  $m=1$  coefficient would barely be distinguishable from that of  $m=0$  if it were plotted on the figure. The temperature-averaged rate coefficients for  $m=0$  and 1 are compared in Table VI. Although there are no measurements of the elastic scattering rates for Sr  $^1P_1$  + Ar, there is an experimental determination of the elastic  $k_C$  for Sr  $^3P_1$  + Ar.<sup>71</sup> The measured value,  $4.2 \times 10^{-9}$   $\text{cm}^3\text{sec}^{-1}$  at  $T=400^\circ\text{C}$  (673 K), is close to our calculated value for Sr  $^1P_1$  + Ar,  $4.4 \times 10^{-9}$   $\text{cm}^3\text{sec}^{-1}$ . Our calculated value is probably fairly reliable, since the same potentials lead to good agreement with the impact-broadening rate and alignment-destruction rate. The similarity of elastic scattering rates for Sr  $^1P_1$  and  $^3P_1$  + Ar is not surprising when we consider that the same experiment<sup>71</sup> found Sr  $^3P_1$  + Ar alignment-destruction rates which agreed with those of Alford *et al.*<sup>2</sup> for Sr  $^1P_1$  + Ar within the error bars of both experiments.

## V. CONCLUSION

We have demonstrated through specific numerical calculations how radiative scattering theory provides a practical tool for giving a unified treatment of weak-field atomic line broadening and redistribution phenomena. The theory gives a complete description of an isolated binary collision in a radiation field, including the simultaneous influence of radiative and inelastic collisional interactions. The theory can be applied to optical collisions for detunings throughout the absorption profile, from the impact core to the far wings. The Sr + Ar system provides a useful prototype that has been well studied experimentally and is amenable to theoretical calculation. The  $^1P \leftarrow ^1S$  transition is the simplest realistic atomic system which exhibits effects of atomic degeneracy. We have tried to project a maximum amount of experimentally observable information from our calculations. Generally,

the comparison of calculated and measured results are favorable when the adjusted potentials are used. When data have been lacking for Sr + Ar, we have described how our results are compatible with results on closely related systems.

Our attempt to obtain potentials for SrAr is fraught with difficulties, and it is not possible to assess with any confidence how reliable our adjusted potentials are. There is still a clear need for further theoretical and/or experimental study of the Group II rare-gas potentials. There are no experimental spectroscopic studies of these species as for the analogous NaNe molecule.<sup>73</sup> Such studies should be well within the capability of modern technology. An improved theoretical "supermolecule" calculation along the lines of Saxon, Olson, and Liu<sup>55</sup> for NaAr, which simultaneously calculates the exchange-overlap and dispersion contributions to the energy, should be possible, either with *ab initio* or pseudopotential techniques.

Since this paper has concentrated on describing a variety of numerical results, we have not given here any detailed interpretive analysis of these results. There are two distinct regions of detuning, each corresponding to a quite different physical picture of absorption: the impact region for small detunings where  $\Delta/\hbar \ll \tau_c^{-1}$ , and the line wings for large detunings where the inequality in this condition is reversed. We will describe in separate papers the general radiative scattering theory and analysis of these two regions.

The impact limit is very familiar in line-broadening theory.<sup>40-42,43</sup> The Franck-Condon integrals in Eq. (13) are expressed in terms of the asymptotic properties of the field-free wave functions of the initial and final states. From the viewpoint of radiative scattering theory the photon may be absorbed at large  $R$  either as the two atoms approach each other or as they separate. If the former, the atoms undergo a complete collision on the excited-state set of potentials; if the latter, they undergo a complete collision on the ground-state set. Thus, there are two independent "whole collision" paths which contribute to an absorption event and therefore interfere. The impact-broadening cross section can thus be expressed in terms of the field-free  $S$  matrices which separately describe ground- and excited-state scattering. There is a coherent contribution due to elastic scattering and an incoherent contribution due to inelastic scattering. Radiative scattering theory does not give any new insights into impact-limit theory, and is not even the most efficient way to do impact-limit calculations. However, our theory has the virtue of ensuring that all inelastic effects are properly included in the radiative scattering cross sections, joins smoothly between impact and far-wing detunings, and can describe departures from the impact limit even for small detuning. For example, we are able to predict the dispersion asymmetry of the Lorentzian absorption profile.

The line-wing region of the profile can further be separated into far- and intermediate-wing regions. Allowed atomic transitions will always involve degenerate asymptotes and multiple molecular Born-Oppenheimer states (since  $S \leftarrow S$  transitions are forbidden). Far-wing absorption can usually be described in terms of adiabatic

Franck-Condon absorption between initial and final isolated Born-Oppenheimer states. Absorption occurs at small  $R$  at one or more stationary phase points where  $\hbar\omega$  equals the difference between upper and lower potentials. The atoms separate on the excited-state potential, and may be influenced as they separate by nonadiabatic or inelastic collisional effects involving coupling to other molecular potentials. This "half-collision" picture of absorption and redistribution can be quantified using a generalized multichannel quantum-defect analysis of the close-coupled wave function.<sup>18,20</sup> For far-wing detuning the radiative scattering amplitudes can often be factored into separate terms representing (1) an initial state half-collision which prepares the molecule for absorption from a specific Born-Oppenheimer state, (2) Franck-Condon excitation, and (3) a final state half-collision which describes the distribution of states of the separated atoms which come from the particular Born-Oppenheimer state excited. Such a theory may be used to show how the simple

geometric model of polarization redistribution of Lewis *et al.*<sup>15</sup> is at least a qualitatively good picture. This theory also aids our understanding of far-wing fine-structure redistribution experiments.<sup>23</sup> On the other hand, the radiative scattering amplitudes for intermediate-wing detuning normally involve interfering contributions from more than one such half-collision path. Although the effects of such interferences can be substantially reduced by summing over many partial waves, the intermediate-wing region is generally much more difficult to interpret than the far wings.

#### ACKNOWLEDGMENTS

The authors wish to thank their colleagues W. Stevens and M. Krauss for advice on the *ab initio* calculations. This work was supported in part by the Air Force Office of Scientific Research under Contract No. AFOSR-ISSA-86-005.

- <sup>1</sup>P. Thomann, K. Burnett, and J. Cooper, *Phys. Rev. Lett.* **45**, 1325 (1980).
- <sup>2</sup>W. J. Alford, K. Burnett, and J. Cooper, *Phys. Rev. A* **27**, 1310 (1983).
- <sup>3</sup>W. J. Alford, N. Andersen, K. Burnett, and J. Cooper, *Phys. Rev. A* **30**, 2366 (1984).
- <sup>4</sup>W. J. Alford, N. Andersen, M. Belsley, J. Cooper, D. M. Warrington, and K. Burnett, *Phys. Rev. A* **31**, 3012 (1985).
- <sup>5</sup>J. L. Carlsten, A. Szoke, and M. G. Raymer, *Phys. Rev. A* **15**, 1029 (1977).
- <sup>6</sup>P. D. Kleiber, K. Burnett, and J. Cooper, *Phys. Lett.* **84A**, 182 (1981).
- <sup>7</sup>J. Cooper, *Astrophys. J.* **228**, 339 (1979).
- <sup>8</sup>G. Nienhuis and F. Schuller, *Physica* **92C**, 397 (1977).
- <sup>9</sup>G. Nienhuis, *Physica* **93C**, 393 (1978); **95C**, 266 (1978); *J. Phys. B* **16**, 1 (1983).
- <sup>10</sup>J. Copper, R. J. Ballagh, and K. Burnett, *Phys. Rev. A* **22**, 535 (1980).
- <sup>11</sup>J. Cooper and K. Burnett, *Phys. Rev. A* **22**, 2027; **22**, 2044 (1980).
- <sup>12</sup>P. S. Julienne, in *Spectral Line Shapes*, edited by K. Burnett (de Gruyter, Berlin, 1983), Vol. 2, pp. 769–786.
- <sup>13</sup>P. S. Julienne and F. H. Mies, *Phys. Rev. A* **30**, 831 (1984).
- <sup>14</sup>W. Behmenburg, V. Kroop, and F. Reberstrost, *J. Phys. B* **18**, 2693 (1985).
- <sup>15</sup>E. L. Lewis, J. M. Salter, and M. Harris, *J. Phys. B* **14**, L173 (1981); E. L. Lewis, M. Harris, W. J. Alford, J. Cooper, and K. Burnett, *J. Phys. B* **16**, 553 (1983).
- <sup>16</sup>J. Cooper, in *Spectral Line Shapes*, edited by K. Burnett (de Gruyter, Berlin, 1983), Vol. 2, pp. 737–754.
- <sup>17</sup>K. Burnett, in *Electron and Atomic Physics*, edited by J. Eichler, I. V. Hertel, and N. Stolterfoht (North-Holland, Amsterdam, 1984), pp. 649–660.
- <sup>18</sup>F. H. Mies and P. S. Julienne, in *Spectral Line Shapes*, edited by F. Rostas (de Gruyter, Berlin, 1985), Vol. 3, pp. 393–420.
- <sup>19</sup>P. S. Julienne and F. H. Mies, in *Spectral Line Shapes*, edited by F. Rostas (de Gruyter, Berlin, 1985), Vol. 3, pp. 525–526.
- <sup>20</sup>P. S. Julienne and F. H. Mies, in *Electron and Atomic Collisions*, edited by D. C. Lorents, W. E. Meyerhof, and J. R. Petersen (Elsevier, Amsterdam, to be published).
- <sup>21</sup>K. Burnett, *Phys. Rep.* **118**, 340 (1985).
- <sup>22</sup>P. S. Julienne and F. H. Mies, in *Proceedings of 10<sup>e</sup> Colloque sur la Physique des Collisions Atomiques et Electroniques, Aussois, France*, edited by N. Sadeghi and J. Berlande, 1984 (unpublished).
- <sup>23</sup>L. Vahala, P. S. Julienne, and M. Havey, *Phys. Rev. A* **34**, 1856 (1986).
- <sup>24</sup>F. H. Mies, in *Theoretical Chemistry: Advances and Perspectives*, edited by D. Henderson (Academic, New York, 1981), Vol. 6B, pp. 127–198.
- <sup>25</sup>I. H. Zimmerman, J. M. Yuan, and T. F. George, *J. Chem. Phys.* **66**, 2638 (1977).
- <sup>26</sup>P. L. DeVries, M. S. Mahlab, and T. F. George, *Phys. Rev. A* **17**, 546 (1978).
- <sup>27</sup>P. L. DeVries and T. F. George, *Mol. Phys.* **36**, 151 (1978); **38**, 561 (1979); *Phys. Rev. A* **18**, 1751 (1978).
- <sup>28</sup>P. S. Julienne, *Phys. Rev. A* **26**, 3299 (1982).
- <sup>29</sup>K. Kulander and F. Reberstrost, *Phys. Rev. Lett.* **51**, 1262 (1983).
- <sup>30</sup>K. Kulander and F. Reberstrost, *J. Chem. Phys.* **80**, 5623 (1984).
- <sup>31</sup>L. Vahala, M. Havey, and P. S. Julienne, in *Spectral Line Shapes*, edited by F. Rostas (de Gruyter, Berlin, 1985), Vol. 3, pp. 527–528.
- <sup>32</sup>E. D. Poliakoff, J. L. Dehmer, D. Dill, A. C. Parr, K. H. Jackson, and R. N. Zare, *Phys. Rev. Lett.* **46**, 907 (1981).
- <sup>33</sup>C. H. Greene and R. N. Zare, *Phys. Rev. A* **25**, 2031 (1982).
- <sup>34</sup>C. H. Greene and R. N. Zare, *Annu. Rev. Phys. Chem.* **33**, 119 (1982).
- <sup>35</sup>J. M. Brown, J. T. Hougen, K. P. Huber, J. W. C. Johns, I. Kopp, H. Lefebvre-Brion, A. J. Merer, D. A. Ramsay, J. Rostas, and R. N. Zare, *J. Mol. Spectrosc.* **55**, 500 (1975).
- <sup>36</sup>F. H. Mies, *Phys. Rev. A* **7**, 942 (1973).
- <sup>37</sup>A. Lurio, R. L. deZafra, and R. J. Goshen, *Phys. Rev.* **134A**, 1198 (1964).
- <sup>38</sup>P. S. Julienne and F. H. Mies, *Phys. Rev. A* **25**, 3399 (1982).
- <sup>39</sup>F. H. Mies, P. S. Julienne, Y. B. Band, and S. Singer, *J. Phys. B* (to be published).
- <sup>40</sup>M. Baranger, *Phys. Rev.* **112**, 855 (1958).
- <sup>41</sup>A. Ben-Reuven, *Phys. Rev.* **145**, 7 (1966).

- <sup>42</sup>R. Shafer and R. G. Gordon, *J. Chem. Phys.* **58**, 5422 (1973).
- <sup>43</sup>H. van Regemorter and N. Feautrier, *J. Phys. B* **18**, 2673 (1985).
- <sup>44</sup>V. S. Lisitsa and S. I. Yakovlenko, *Zh. Eksp. Teor. Fiz.* **68**, 479 (1975) [*Sov. Phys.—JETP* **41**, 233 (1975)].
- <sup>45</sup>A. Corney and J. V. M. McGinley, *J. Phys. B* **14**, 3047 (1981).
- <sup>46</sup>J. Szudy and W. E. Baylis, *J. Quant. Spectrosc. Radiat. Trans.* **15**, 641 (1975).
- <sup>47</sup>J. F. Kielkopf, *J. Phys. B* **13**, 3813 (1980).
- <sup>48</sup>R. E. Walkup, A. Spielfiedel, and D. E. Pritchard, *Phys. Rev. Lett.* **45**, 986 (1980).
- <sup>49</sup>M. Harris, E. L. Lewis, D. McHugh, and I. Shannon, *J. Phys. B* **17**, L661 (1984).
- <sup>50</sup>J. Szudy and W. E. Baylis, *J. Quant. Spectrosc. Radiat. Transfer* **17**, 269 (1977); **17**, 681 (1977).
- <sup>51</sup>E. L. Lewis, *Phys. Rep.* **58**, 1 (1980).
- <sup>52</sup>G. Grawert, *Z. Phys.* **225**, 283 (1969).
- <sup>53</sup>P. R. Berman and W. E. Lamb, *Phys. Rev.* **187**, 221 (1969).
- <sup>54</sup>J. Pascale, in *Spectral Line Shapes*, edited by F. Rostas (de Gruyter, Berlin, 1985), Vol. 3, pp. 563–586.
- <sup>55</sup>R. P. Saxon, R. E. Olson, and B. Liu, *J. Chem. Phys.* **67**, 2692 (1977).
- <sup>56</sup>A. Koide, *J. Phys. B* **9**, 3173 (1976).
- <sup>57</sup>M. Krauss and D. B. Neumann, *J. Chem. Phys.* **71**, 107 (1979).
- <sup>58</sup>K. T. Tang, J. M. Norbeck, and P. R. Certain, *J. Chem. Phys.* **64**, 3063 (1976).
- <sup>59</sup>H. L. Swartz, T. M. Miller, and B. Bederson, *Phys. Rev. A* **10**, 1924 (1974).
- <sup>60</sup>W. Mueller, J. Flesch, and W. Meyer, *J. Chem. Phys.* **80**, 3297 (1984); W. Mueller and W. Meyer, *ibid.* **80**, 3311 (1984).
- <sup>61</sup>G. D. Mahan, *J. Chem. Phys.* **48**, 950 (1968); **50**, 2755 (1969).
- <sup>62</sup>T. R. Proctor and W. C. Stwally, *J. Chem. Phys.* **66**, 2063 (1977).
- <sup>63</sup>J. P. Desclaux, *At. Data* **12**, 311 (1973).
- <sup>64</sup>R. A. Gordon, *J. Chem. Phys.* **51**, 14 (1969).
- <sup>65</sup>R. E. M. Hedges, D. L. Drummond, and A. Gallagher, *Phys. Rev. A* **6**, 1519 (1972).
- <sup>66</sup>G. Herzberg, *Molecular Spectra and Molecular Structure I. Spectra of Diatomic Molecules* (van Nostrand, Princeton, 1950), p. 208.
- <sup>67</sup>H. Harima, Y. Fukuzo, K. Tachibana, and Y. Urano, *J. Phys. B* **14**, 3069 (1981).
- <sup>68</sup>J. M. Farr and W. R. Hindmarsh, *J. Phys. B* **4**, 568 (1971).
- <sup>69</sup>N. P. Penkin and L. N. Shabanova, *Opt. Spektrosk.* **25**, 795 (1968).
- <sup>70</sup>H. Harima, K. Tachibana, and Y. Urano, *J. Phys. B* **15**, 3679 (1982).
- <sup>71</sup>M. Saidi, thesis, University of Tunis, Tunis, Tunisia, 1985.
- <sup>72</sup>J. C. Keller and J. L. Le Gouet, *Phys. Rev. A* **32**, 1624 (1985).
- <sup>73</sup>W. P. Lapatovich, R. Ahmad-Bitar, P. E. Moskowitz, I. Renhorn, R. A. Gottscho, and D. E. Pritchard, *J. Chem. Phys.* **73**, 5419 (1980); R. A. Gottscho, R. Ahmad-Bitar, W. P. Lapatovich, I. Renhorn, and D. E. Pritchard, *ibid.* **75**, 2546 (1981).